JPET Fast Forward. Published on September 27, 2020 as DOI: 10.1124/jpet.120.000235
This article has not been copyedited and formatted. The final version may differ from this version.

Title:

Interaction of halogenated tyrosine/phenylalanine-derivatives with Organic Anion Transporter (OAT) 1 in the renal handling of tumor imaging probes

Authors:

Chunhuan Jin, Ling Wei, Ryuichi Ohgaki, Hideyuki Tominaga, Minhui Xu, Suguru Okuda, Hiroki Okanishi, Yasuharu Kawamoto[1], Xin He, Shushi Nagamori, and Yoshikatsu Kanai

Authors' affiliations:

Department of Bio-system Pharmacology, Graduate School of Medicine, Osaka University, Osaka, Japan (C.J., L.W., R.O., M.X., Ya.K., S.O., H.O., Yo.K.); Integrated Frontier Research for Medical Science Division, Institute for Open and Transdisciplinary Research Initiative (OTRI), Osaka University (Yo.K.); Department of Oncology Clinical Development, Gunma University Graduate School of Medicine, Maebashi, Gunma, Japan (H.T.); School of Traditional Chinese Medicine, Guangdong Pharmaceutical University, Guangzhou, Guangdong, China (L.W., X.H.); Department of Collaborative Research for Bio-Molecular Dynamics, Nara Medical University, Nara, Japan (S.N.)

JPET Fast Forward. Published on September 27, 2020 as DOI: 10.1124/jpet.120.000235
This article has not been copyedited and formatted. The final version may differ from this version.

Running title:

Halogenated-tyrosine probes interact with renal transporter

Address correspondence to:

Dr. Yoshikatsu Kanai

Department of Bio-system Pharmacology, Graduate School of Medicine, Osaka University, 2-2 Yamadaoka, Suita, Osaka 565-0871, Japan.

Tel: +81-6-6879-3521; Fax: +81-6-6879-3529

E-mail: ykanai@pharma1.med.osaka-u.ac.jp

The number of text pages: 53

The number of tables: 2

The number of figures: 8

The number of references: 35

The number of words in Abstract: 250

The number of words in Introduction: 545

The number of words in Discussion: 1499

JPET Fast Forward. Published on September 27, 2020 as DOI: 10.1124/jpet.120.000235
This article has not been copyedited and formatted. The final version may differ from this version.

Abbreviations:

AMT (L-α-methyl-tyrosine), DOX (Doxycycline), 3-F-AMP ((S)-α-methyl-3-fluorophenylalanine), FAMT (3-fluoro-α-methyl-L-tyrosine), 2-FAMT (2-fluoro-α-methyl-L-tyrosine), [^{18}F]FDG (2-^{18}F-fluoro-2-deoxy-D-glucose), 2-F-*m*-Tyr (2-fluoro-*meta*-tyrosine), 4-F-*m*-Tyr (4-fluoro-*meta*-tyrosine), 5-F-*m*-Tyr (5-fluoro-*meta*-tyrosine), 6-F-*m*-Tyr (6-fluoro-*meta*-tyrosine), 3-F-*o*-Tyr (3-fluoro-*ortho*-tyrosine), 4-F-*o*-Tyr (4-fluoro-*ortho*-tyrosine), 5-F-*o*-Tyr (5-fluoro-*ortho*-tyrosine), 6-F-*o*-Tyr (6-fluoro-*ortho*-tyrosine), 2-FT (2-fluoro-tyrosine), 3-FT (3-fluoro-tyrosine), HBSS (Hank's balanced salt solution), 3-I-AMP ((S)-α-methyl-3-iodophenylalanine), IMT (3-iodo-α-methyl-L-tyrosine), 4-I-*m*-Tyr (4-iodo-L-*meta*-tyrosine), 2-IT (2-iodo-L-tyrosine), 3-IT (3-iodo-L-tyrosine), LAT1 (L-type amino acid transporter 1), OAT1 (organic anion transporter 1), PAH (*p*-aminohippuric acid), PET (positron emission tomography), SPECT (single-photon emission computed tomography).

Recommended section assignment:

Metabolism, Transport, and Pharmacogenomics

JPET Fast Forward. Published on September 27, 2020 as DOI: 10.1124/jpet.120.000235
This article has not been copyedited and formatted. The final version may differ from this version.

Abstract

Halogenated tyrosine/phenylalanine derivatives have been developed for use in tumor imaging and targeted alpha therapy. 3-Fluoro-α-methyl-L-tyrosine (FAMT), targeting amino acid transporter LAT1 (SLC7A5), is a cancer-specific positron-emission-tomography probe yet exhibits high renal accumulation supposed to be mediated by organic anion transporter OAT1 (SLC22A6). In the present study, we investigated the structural requirements of FAMT essential for interaction with OAT1. OAT1 transported FAMT with a K_m of 171.9 μM. In structure–activity relationship analyses, removal of either the 3-halogen or 4-hydroxyl group from FAMT or its structural analog 3-iodo-α-methyl-L-tyrosine greatly decreased the interaction with OAT1, reducing the ^{14}C-*p*-aminohyppurate uptake inhibition and the efflux induction. By contrast, the α-methyl group, which is essential for LAT1-specificity, contributed to a lesser degree. In fluorinated tyrosine derivatives, fluorine at any position was accepted by OAT1 when there was a hydroxyl group at the *ortho*-position, whereas *ortho*-fluorine was less interactive when a hydroxyl group was at *meta*- or *para*-position. The replacement of the *ortho*-fluorine with a bulky iodine atom greatly increased the interaction. In *in vivo* studies, probenecid decreased the renal accumulation ($p < 0.001$) and urinary excretion ($p = 0.0012$) of FAMT, whereas the plasma concentration was increased, suggesting the

JPET Fast Forward. Published on September 27, 2020 as DOI: 10.1124/jpet.120.000235
This article has not been copyedited and formatted. The final version may differ from this version.

involvement of OAT1-mediated trans-epithelial organic anion excretion. LAT1-specific 2-fluoro-α-methyl-tyrosine, which had lower affinity for OAT1, exhibited lower renal accumulation (p = 0.0142) and higher tumor uptake (p = 0.0192) compared with FAMT. These results would provide a basis to design tumor specific compounds that can avoid renal accumulation for tumor imaging and targeted alpha therapy.

Significance Statement:

We revealed the structural characteristics of halogenated tyrosine derivatives used as tumor-imaging probes essential for interaction with the organic anion transporter responsible for their renal accumulation. We have confirmed that such interactions are important for renal handling and tumor uptake. The critical contribution of hydroxyl and halogen groups and their positions, as well as the role of α-methyl group found in the present study may facilitate the development of tumor-specific compounds while avoiding renal accumulation for use in tumor imaging and targeted-alpha-therapy.

JPET Fast Forward. Published on September 27, 2020 as DOI: 10.1124/jpet.120.000235
This article has not been copyedited and formatted. The final version may differ from this version.

Introduction

Halogenated aromatic amino acid derivatives have been developed for potential use as tracers in positron emission tomography (PET) and single-photon emission computed tomography (SPECT) for the clinical diagnosis of malignant tumors (Jager et al., 2001; Plathow and Weber, 2008). Amino acid probes are advantageous in cancer diagnosis due to their cancer specificity, which could overcome the issues of false positives and high physiological backgrounds in conventionally used 2-^{18}F-fluoro-2-deoxy-D-glucose ([^{18}F]FDG)-PET imaging (Cook et al.,1999). We have previously reported that the halogenated tyrosine derivatives, 3-fluoro-α-methyl-L-tyrosine (FAMT) and 3-iodo-α-methyl-L-tyrosine (IMT), used as cancer-specific probes for PET and SPECT, respectively, are highly specific to LAT1 (SLC7A5) among amino acid transporters (Wiriyasermkul et al., 2012; Wei et al., 2016b). LAT1 is an amino acid transporter predominantly expressed in primary tumors of various tissue origins and their metastatic lesions (Kandasamy et al., 2018). LAT1 primarily transports branched-chain and aromatic amino acids and their derivatives (Kanai et al., 1998; Uchino et al., 2002). The LAT1 specificity of FAMT and IMT is due to their α-methyl groups (Wiriyasermkul et al., 2012).

In [^{18}F]FAMT-PET and [^{123}I]IMT-SPECT imaging, the kidney is the only organ that demonstrates high physiological uptake, which limits the use of these compounds for

JPET Fast Forward. Published on September 27, 2020 as DOI: 10.1124/jpet.120.000235
This article has not been copyedited and formatted. The final version may differ from this version.

imaging of abdominal tumors (Suzuki et al., 2014; Shikano et al., 2004b). Based on the effects of organic anion transporter inhibitors such as probenecid, it has been proposed that the renal accumulation of IMT is mediated by the accumulative trans-epithelial organic anion excretion pathway in the S2 segment of renal proximal tubules (Shikano et al., 2004b; Nakajima et al, 2007). Because FAMT and IMT are structurally identical except for the fluorine/iodine substitution at position 3 of the benzene ring, we hypothesized that the renal handling of FAMT could be similar to that of IMT and sought to determine which renal transporters transport FAMT. Among organic ion transporters involved in the uptake into tubular epithelial cells, we reported that the transporters OAT1 (SLC22A6) in the basolateral membrane and OAT10 (SLC22A13) and OCTN2 (SLC22A5) in the apical membrane could transport FAMT (Wei et al., 2016a). Among them, OAT1 is a transporter involved in the accumulative trans-epithelial organic anion excretion pathway (Anzai et al., 2006).

In the present study, we examined the interaction of FAMT and its related compounds with OAT1 to reveal the structural characteristics of FAMT essential for interaction with OAT1 and finally identified the halogenated compounds with low affinity for OAT1 yet high specificity for LAT1. We furthermore conducted *in vivo* studies to evaluate the relevance of OAT1 in the renal handling of FAMT and its related compounds, as well as

JPET Fast Forward. Published on September 27, 2020 as DOI: 10.1124/jpet.120.000235
This article has not been copyedited and formatted. The final version may differ from this version.

their tumor accumulation. The structure–activity relationship analysis in the present study was designed based on reports showing that 4-iodo-L-*meta*-tyrosine (4-I-*m*-Tyr), which has differences in halogen, hydroxyl and α-methyl groups compared with IMT/FAMT (Figure 1), targeted LAT1 similar to IMT/FAMT, yet exhibited decreased renal accumulation (Shikano et al., 2003). Using a series of halogenated tyrosine/phenylalanine derivatives, we report that the presence and/or relative positions of halogen, hydroxyl, and α-methyl groups are critical for interaction with OAT1. The results of the present study provide a basis to design tumor-specific compounds that avoid renal accumulation for tumor imaging. Such compounds would also be beneficial for efficient targeted alpha therapy targeting LAT1 while avoiding renal damage (Watabe et al., 2020).

JPET Fast Forward. Published on September 27, 2020 as DOI: 10.1124/jpet.120.000235
This article has not been copyedited and formatted. The final version may differ from this version.

Materials and Methods

Materials

FAMT and 2-fluoro-L-α-methyl-tyrosine (2-FAMT) were obtained from Nard Institute, Ltd. (Amagasaki, Japan) (Wiriyaserumkul et al., 2012). ^{14}C-FAMT (1.77 GBq/mmol) was obtained from Sekisui Medical (Tokyo, Japan) (Wei et al., 2016a). ^{14}C-*p*-Aminohippurate (PAH) (1.931 GBq/mmol) was purchased from Moravek Biochemicals (Brea, CA). Standard amino acids and L-α-methyl-tyrosine (AMT) were purchased from Sigma-Aldrich (St Louis, MO). IMT was obtained from Advance Bio-chemical Compounds GmbH (Radeberg, Germany). 3-Fluoro-L-tyrosine (3-FT) was purchased from Tokyo Chemical Industry (Tokyo, Japan). Unless specially denoted, other chemicals and cell media were purchased from Wako Pure Chemical Industries (Osaka, Japan). The chemical structures of compounds used in the present study are presented in Figure 1.

Establishment of a stable OAT1-expressing cell line

A stable cell line of doxycycline-inducible expression of human OAT1 was constructed. The coding sequence of human OAT1 (GenBank Accession: AB009697.1) was amplified by PCR from pcDNA3.1(+)-hOAT1 (Ichida et al., 2003) using the primer

JPET Fast Forward. Published on September 27, 2020 as DOI: 10.1124/jpet.120.000235
This article has not been copyedited and formatted. The final version may differ from this version.

pair forward 5′-CGGGATCCATGGCCTTTAATGACCTCCTG-3′, and reverse 5′-CTCCTCGAGTCAGAGTCCATTCTTCTCTTG-3′. The amplified fragment was digested by *Bam*H I and *Xho* I and ligated into the pcDNA5/FRT/TO vector (Invitrogen, Carlsbad, CA) at *Bam*H I and *Xho* I sites to obtain pcDNA5/FRT/TO-hOAT1.

Flp-In T-Rex-293 cells (Nagamori et al., 2016) were cultured in Dulbecco's modified Eagle medium (DMEM, Wako Pure Chemical Industries, Osaka, Japan) supplemented with 10% fetal bovine serum (FBS, Gibco, Grand Island, NY) and 1% (v/v) penicillin-streptomycin solution (Nakalai Tesque, Kyoto, Japan). Flp-In T-REx 293 cells were transfected and screened with pcDNA5/FRT/TO-hOAT1 as described previously (Nagamori et al., 2016) with a minor modification. Two days after transfection, the cells were passaged. After cells attached, the growth medium was replaced with selection media containing 100 μg/mL hygromycin B (Nakalai Tesque, Kyoto, Japan) and 5 μg/mL blasticidin (Invitrogen, Carlsbad, CA). The selection medium was changed every 3 to 4 days until the desired number of cells were grown. The cell colonies were examined by RT-PCR for the expression of human OAT1. A positive cell line, designated FlpIn293-TetR-hOAT1, was functionally confirmed by the uptake of ^{14}C-PAH (see below) and used for the present study.

JPET Fast Forward. Published on September 27, 2020 as DOI: 10.1124/jpet.120.000235
This article has not been copyedited and formatted. The final version may differ from this version.

Cell Culture

FlpIn293-TetR-OAT1 cells with inducible human OAT1 expression (Tet-On) were cultured in DMEM supplemented with FBS (10%), penicillin–streptomycin (1%), hygromycin B (100 μg/mL), and blasticidin (5 μg/mL) in a humidified incubator at 37°C supplied with 5% CO_2. Forty-eight hours before uptake/efflux experiments, cells were seeded on poly-D-lysine-coated 24 well plates at a density of 1.5 $\times 10^5$ cells/well, with or without 1μg/mL doxycycline (Dox).

Uptake Measurements and Inhibition Experiments

Uptake measurements were conducted as described previously (Ohgaki et al., 2016). The uptake of ^{14}C-PAH and ^{14}C-FAMT by cells was measured for 1 min or indicated time periods in Na^+-free Hanks balanced salt solution ([HBSS]: 125 mM choline chloride, 4.8 mM KCl, 1.2 mM $MgSO_4$, 1.2 mM KH_2PO_4, 1.3 mM $CaCl_2$, 5.6 mM D-glucose, and 25 mM MES, pH 7.4). After uptake was terminated, the cells were lysed and the radioactivity measured using a β-scintillation counter (LSC-3100, Aloka, Tokyo, Japan). The protein concentrations of cell lysates were determined using a Micro BCA Protein Assay Kit (Thermo Fisher Scientific, Rockford, IL). OAT1-mediated uptake was calculated by

JPET Fast Forward. Published on September 27, 2020 as DOI: 10.1124/jpet.120.000235
This article has not been copyedited and formatted. The final version may differ from this version.

subtracting the uptake value without Dox treatment from that with Dox treatment. To determine kinetic parameters, OAT1-mediated ^{14}C-FAMT uptake was plotted against FAMT concentration and fitted to a Michaelis–Menten curve. The Michaelis constant (K_m), the maximal uptake rate (V_{max}), and Eadie–Hofstee plot were obtained using the enzyme kinetics module of GraphPad Prism 7 (GraphPad Software Inc., San Jose, CA). Kinetic data are summarized in Table 1.

For inhibition experiments, OAT1-mediated uptake of ^{14}C-PAH (1 μM), a typical substrate of OAT1, was measured for 1 min with or without non-radiolabeled test compounds at the indicated concentrations. The half-maximal inhibitory effect (IC_{50}) of each compound was determined by experiments in which OAT1-mediated uptake of ^{14}C-PAH (1 μM) was measured for 1 min in the presence of the compound at concentrations of 1, 3, 10, 30, 100, 300, 1000 and 3000 μM. IC_{50} values were obtained by fitting the data to inhibition curves using nonlinear regression analysis in GraphPad Prism 7 (GraphPad Software Inc.). IC_{50} values obtained by inhibition experiments are summarized in Table 1.

Efflux Measurements

Efflux measurements were conducted as described previously (Wiriyaserumkul

JPET Fast Forward. Published on September 27, 2020 as DOI: 10.1124/jpet.120.000235
This article has not been copyedited and formatted. The final version may differ from this version.

et al., 2012; Shiraya et al., 2010). The cells were preloaded with ^{14}C-PAH for 10 min in Na^+-free HBSS containing 100 μM ^{14}C-PAH (1.931 MBq/mmol) via OAT1-mediated uptake. After washing the cells with Na^+-free HBSS three times, the efflux was initiated by changing the medium to Na^+-free HBSS with or without the indicated concentrations of non-radiolabeled test compounds, and measured for 1 min. The medium was then collected, and the radioactivity in the medium and the remaining radioactivity in the cells were counted. ^{14}C-PAH efflux was expressed as a percentage of total radioactivity (the radioactivity of the medium divided by the sum of the radioactivity of the medium and the remaining radioactivity in cells). The ^{14}C-PAH efflux induced by test compounds was calculated by subtracting the ^{14}C-PAH efflux in the absence of the test compounds from that in the presence of test compounds.

The kinetic parameters of test compounds in the induction of ^{14}C-PAH efflux were determined at the concentrations of 1, 3, 10, 30, 100, 300, and 1,000 μM. The ^{14}C-PAH efflux induced by test compounds was plotted against the concentration of the compounds and fitted to a Michaelis–Menten curve. K_m and V_{max} were determined using an Eadie–Hofstee plot. The K_m values obtained are summarized in Table 1.

Tissue Accumulation and Urinary Excretion Studies

Animal experiments were conducted with approval according to the regulations of

JPET Fast Forward. Published on September 27, 2020 as DOI: 10.1124/jpet.120.000235
This article has not been copyedited and formatted. The final version may differ from this version.

the Animal Care and Use Committee of Osaka University.

To examine the effects of probenecid on renal accumulation, plasma concentration, and urinary excretion of FAMT, male ddY mice (4–6 weeks, 20–25 g) were intravenously administered FAMT (1.5 mg/kg) in 0.1 mL saline (0.9% NaCl) from the tail vein. Probenecid (50 mg/kg) in 0.1 mL saline was pre-administered through the tail vein 10 min before the injection of FAMT. Ten minutes after the administration of FAMT, mice were anesthetized by intraperitoneal injection of three types of mixed anesthetic agents (0.3 mg/kg of medetomidine, 4.0 mg/kg of midazolam, and 5.0 mg/kg of butorphanol in saline), and fresh urine was collected by puncture of the bladder. The animals were euthanized under deep anesthesia, and kidneys were dissected out and weighed. After rinsed in phosphate-buffered saline (PBS), the kidneys were stored at −80 °C for HPLC analysis. Blood was taken at the same time by cardiac puncture, into tubes containing sodium citrate solution (3.2%, 25 μL). Blood samples were centrifuged at 2,000 × g at 4°C for 15 min. The obtained plasma was adjusted to 1 mL with deionized water and stored at −80°C.

For the comparison of the renal accumulation, plasma concentration, and urinary excretion of FAMT, 2-FAMT, and 2-FT, male ddY mice (4–6 weeks, 25–30 g) were administered equimolar amounts of FAMT (1.5 mg/kg), 2-FAMT (1.5 mg/kg), or 2-FT (1.4 mg/kg) in 0.1 mL saline (0.9% NaCl) intravenously from the tail vein. Ten

JPET Fast Forward. Published on September 27, 2020 as DOI: 10.1124/jpet.120.000235
This article has not been copyedited and formatted. The final version may differ from this version.

minutes after administration, kidneys, blood, and urine were collected and processed as described above.

To compare the accumulation of FAMT and 2-FAMT in tumors, tumor-bearing mice were prepared by inoculating B16F10 mouse melanoma cells (1×10^5 cells/head) into the back of male C57BL/6J mice (5–6 weeks, 18–22 g). When palpable tumors developed (~10 mm in diameter), mice were administrated FAMT (1.5 mg/kg) or 2-FAMT (1.5 mg/kg) in 0.1 mL saline (0.9% NaCl) intravenously via the tail vein. At 10 min or 1 h after injection, mice were anesthetized and sacrificed as described above. Tumors and the kidney and skeletal muscle were dissected.

Pharmacokinetic Studies in Mice

To determine pharmacokinetic parameters of FAMT and 2-FAMT, kidneys, blood and urine were collected at different time points (10 min, 30 min, 1 h, 2 h and 3 h) after the intravenous administration of FAMT (1.5 mg/kg) or 2-FAMT (1.5 mg/kg) in ddY mice and processed as described above. Pharmacokinetic parameters were calculated by means of the noncompartmental analysis (WinNonlin, version 8.1.0, Pharsight, Mountain View, CA). The area under the plasma concentration-time curve from 0 to infinity ($AUC_{0-\infty}$), and the elimination rate constant (K_e) were calculated by a nonlinear least-squares method.

JPET Fast Forward. Published on September 27, 2020 as DOI: 10.1124/jpet.120.000235
This article has not been copyedited and formatted. The final version may differ from this version.

The renal clearance (CL_{renal}) was calculated by dividing the amount of compound excreted into urine ($Ae_{0-\infty}$) by $AUC_{0-\infty}$. (Imaoka et al., 2007).

Protein binding assays

Protein biding assays for FAMT and 2-FAMT were conducted in terms of plasma protein binding and tumor-tissue protein binding using the plasma and tumors obtained from B16F10 tumor-bearing C57BL/6J mice prepared as described above. Plasma protein binding assay was performed as described previously (Ohshima et al., 2013). Twenty microliter solution of FAMT or 2-FAMT (50 nmol per milliliter saline) was added to 180 μL of freshly prepared plasma to make up the final concentration of 5 nmol per milliliter, which was close to the plasma concentration as well as the concentration in tumor (the amount of the compound per gram of tumor tissue) at 1 h after the intravenous administration. Then, the samples were incubated at 37 °C for 1 h and filtered through a 10-kDa Amicon® Ultra Centrifugal tube (Merck Millipore Ltd., Ireland). The amount of unbound FAMT and 2-FAMT was analyzed by HPLC as described below. The protein-unbound free compound fraction (f_u) was expressed as a percentage of free compound to the total amount in the sample. For tumor protein binding, tumors were homogenized by adding saline with the volume ratio of 1:4 (1 volume of tumor with 4

JPET Fast Forward. Published on September 27, 2020 as DOI: 10.1124/jpet.120.000235
This article has not been copyedited and formatted. The final version may differ from this version.

volume of saline) on ice. The homogenate was processed same as the plasma described above and f_u was obtained for FAMT and 2-FAMT.

High-performance liquid chromatography analysis

Urine and tissue samples were measured using HPLC. Urine samples were adjusted to a volume of 200 μL with PBS. Kidney samples were homogenized on ice using a Physcotron NS-310E II (Microtec, Chiba, Japan) in PBS, and the volume was adjusted to 1000 μL. After filtering with a syringe filter (0.45μm), the samples (10 μL) were vigorously mixed with 190 μL methanol for deproteinization and centrifuged at 15,000 × *g* at 4°C for 30 min. The supernatant (100 μL) was transferred and dried in a vacuum chamber. The sediment was reconstituted in 20 μL of 200 μM sodium borate (pH 8.0). For fluorescence derivatization, 5 μL of 40 mM 4-fluoro-7-nitro-2,1,3-benzoxadiazole in acetonitrile was added, and samples were heated at 60°C for 2 min as described previously (Wongthai et al., 2015). Derivatization reactions were terminated by adding 75 μL of 0.5% trifluoroacetic acid aqueous solution. Ten microliters of each sample were separated by a NANOSPACE SI-2 HPLC system (Shiseido, Tokyo, Japan) with a fluorescence detector. The analytical column was Capcell Pak C_{18} MGII S5 (250 × 2.0 mm i.d.). The mobile phase was acetonitrile–trifluoroacetic acid–water (27.5:0.05:72.5, v/v/v), with a flow rate

JPET Fast Forward. Published on September 27, 2020 as DOI: 10.1124/jpet.120.000235
This article has not been copyedited and formatted. The final version may differ from this version.

of 200 μL/min. Isocratic elution was conducted for 60 min. The compounds in samples were quantified by comparing the peak height with that of a standard of a known amount. The content of the compounds was expressed as a percentage of injected dose normalized per gram of tissue (wet weight).

Statistical Analysis

All experiments were conducted in four replicates. The data are expressed as means ± SD. Statistical differences were determined using the unpaired Student's *t* test (two sets of data), or one-way analysis of variance (ANOVA) with Dunnett's post-test (more than two sets of data, multiple-to-one comparisons). One-way analysis of variance (ANOVA) with Tukey's honestly significant difference was used for comparisons of differences among groups. Differences were considered significant at $p < 0.05$.

JPET Fast Forward. Published on September 27, 2020 as DOI: 10.1124/jpet.120.000235
This article has not been copyedited and formatted. The final version may differ from this version.

Results

Characterization of OAT1-mediated transport in the stable cell line

To examine the interaction of FAMT-related compounds with OAT1, we established a cell line, FlpIn293-TetR-hOAT1, expressing human OAT1 (hereafter referred to as "OAT1 cells"). OAT1 cells exhibited ^{14}C-PAH uptake dependent on Dox treatment, confirming the functional expression of human OAT1 (Supplemental Fig. 1A). The difference between the uptake with and without Dox treatment was calculated to be OAT1-mediated uptake. Because the ^{14}C-PAH uptake showed a linear dependence on the incubation time up to 5 min (Supplemental Fig. 1B), uptake was measured for 1 min in all subsequent experiments.

To examine whether test compounds were transported by OAT1, we conducted efflux experiments by taking advantage of the obligatory exchanger property of OAT1. Because OAT1 mediates hetero- or homo-substrate exchange of its substrates (Sekine et al., 1997; Apiwattanakul et al., 1999), extracellular PAH induced the efflux of preloaded ^{14}C-PAH in OAT1 cells; ^{14}C-PAH released from cells was higher in the presence of extracellular PAH than that in its absence (Supplemental Fig. 1C). To confirm that ^{14}C-PAH efflux induced by extracellular OAT1-substrates was actually mediated by OAT1 in the established cell line, we preloaded equivalent amounts of ^{14}C-PAH into OAT1-expressing cells and

JPET Fast Forward. Published on September 27, 2020 as DOI: 10.1124/jpet.120.000235
This article has not been copyedited and formatted. The final version may differ from this version.

non-expressing cells, and compared the efflux of ^{14}C-PAH induced by extracellular PAH. Equivalent preloading of ^{14}C-PAH in OAT1-expressing (Dox (+)) and non-expressing (Dox (−)) cells was obtained by incubating the cells with ^{14}C-PAH at the concentrations predetermined individually for Dox (+) and Dox (−) cells (Supplemental Fig. 2A–B). As depicted in Supplemental Fig. 2C, extracellular PAH induced substantial efflux of preloaded ^{14}C-PAH in Dox (+) cells, whereas PAH did not induce efflux in Dox (−) cells. This confirmed that the efflux of ^{14}C-PAH induced by extracellular PAH was mediated by OAT1.

OAT1-mediated ^{14}C-FAMT transport

The interaction of FAMT with OAT1 was first examined in the inhibition experiment in which the uptake of ^{14}C-PAH (1μM) was measured in the presence of various concentrations of FAMT. As shown in Fig. 2A, FAMT inhibited OAT1-mediated ^{14}C-PAH uptake concentration-dependently, with a IC_{50} value listed in Table 1. Then, the transport of FAMT was evaluated by efflux experiments. FAMT concentration-dependently induced the efflux of ^{14}C-PAH preloaded into the cells, suggesting that extracellular FAMT is transported by OAT1 in exchange for preloaded ^{14}C-PAH (Fig. 2B). The transport of FAMT was confirmed by direct

JPET Fast Forward. Published on September 27, 2020 as DOI: 10.1124/jpet.120.000235
This article has not been copyedited and formatted. The final version may differ from this version.

transport assay using ^{14}C-FAMT. ^{14}C-FAMT was transported by OAT1 with a K_m value of 171.9 ± 16.6 μM (n = 4) (Fig. 2C).

Interactions of IMT and 4-I-m-Tyr with OAT1

The interactions of IMT and 4-I-*m*-Tyr with OAT1 was studied in inhibition and efflux experiments. Both compounds inhibited OAT1-mediated ^{14}C-PAH uptake in OAT1 cells concentration-dependently, although IMT showed ~6-fold lower IC_{50} compared with 4-I-*m*-Tyr (Fig. 3A and Table 1). IMT induced efflux of preloaded ^{14}C-PAH, suggesting that IMT is transported by OAT1 (Fig. 3B). Consistent with the inhibition experiments, a smaller efflux was induced by 4-I-*m*-Tyr as compared with IMT (Fig. 3B).

The roles of α-methyl, hydroxyl and halogen groups of IMT and FAMT in interaction with OAT1

To determine which chemical features of IMT are necessary for interaction with OAT1, the roles of the α-methyl, hydroxyl and halogen groups, which differ between IMT and 4-I-*m*-Tyr, were examined. In the comparisons of IMT with 3-I-AMP and AMT, the removal of either the hydroxyl or halogen group of IMT decreased the magnitude of the inhibition of OAT1-mediated ^{14}C-PAH uptake, as well as the induction of ^{14}C-PAH efflux

JPET Fast Forward. Published on September 27, 2020 as DOI: 10.1124/jpet.120.000235
This article has not been copyedited and formatted. The final version may differ from this version.

mediated by OAT1 (Fig. 4A–B). In the comparison between IMT and 3-IT, the influence of the removal of α-methyl group of IMT was smaller than that of the hydroxyl or halogen group on inhibition and efflux (Fig. 4A–B), although it still increased the IC_{50} value by 2.0-fold (Table 1). Similar results were also obtained for FAMT, as the removal of either the hydroxyl or halogen group from FAMT largely reduced the interaction with OAT1 in both inhibition and efflux experiments (the comparisons of FAMT with 3-F-AMP and AMT in Fig. 4C–D). The removal of the α-methyl group from FAMT had also smaller effects than the removal of hydroxyl or halogen group in the comparison between FAMT and 3-FT (Fig. 4C–D), although its removal increased the IC_{50} value by 1.7-fold similar to that of IMT (Table 1).

The positions of the hydroxyl and fluoro groups required for interaction with OAT1

The necessity of the positions of the hydroxyl and halogen groups on the benzene ring for interaction with OAT1 was examined in a series of fluorinated tyrosine regioisomers without an α-methyl group. Because both 3-fluoro and 4-hydroxyl groups were critical (Fig. 4), the 4-hydroxyl group was fixed in the *para*-tyrosine configuration, and the effect of the position of the fluoro group was examined in the first series of experiments. As shown in Fig. 5A–B, the position of

JPET Fast Forward. Published on September 27, 2020 as DOI: 10.1124/jpet.120.000235
This article has not been copyedited and formatted. The final version may differ from this version.

the fluoro group had a large influence on the interaction with OAT1 in both inhibition and efflux experiments. Compared with 3-FT, 2-FT exhibited remarkably decreased inhibition on OAT1-mediated ^{14}C-PAH uptake and decreased induction of ^{14}C-PAH efflux (Fig. 5A–B).

In the second series of experiments, the position of the hydroxyl group was fixed at position 3 (*meta*-tyrosine configuration), and the fluoro group position was altered on the benzene ring. When the fluoro-group was at position 6 on the *meta*-tyrosine, the compound (6-F-*m*-Tyr) exhibited decreased inhibition on OAT1-mediated ^{14}C-PAH uptake, as well as decreased induction of ^{14}C-PAH efflux compared with 2-F-*m*-Tyr, 4-F-*m*-Tyr, and 5-F-*m*-Tyr, which have a fluoro-group at position 2, 4, or 5, respectively (Fig. 5C–D).

In the third series of experiments, the position of the hydroxyl group was fixed at position 2 (*ortho*-tyrosine configuration), and the fluoro-group position was altered on the benzene ring. Compounds with a fluoro group at different positions on *ortho*-tyrosine (3-F-*o*-Tyr, 4-F-*o*-Tyr, 5-F-*o*-Tyr, and 6-F-*o*-Tyr) exhibited similar magnitude of inhibition on OAT1 (Fig. 5E). Consistent with this, all four of these compounds induced OAT1-mediated efflux, although the efflux induced by 4-F-*o*-Tyr was relatively small compared with that induced by the other compounds (Fig. 5F).

JPET Fast Forward. Published on September 27, 2020 as DOI: 10.1124/jpet.120.000235
This article has not been copyedited and formatted. The final version may differ from this version.

Comparison of iodo and fluoro groups in interaction with OAT1

Because IMT exhibited decreased IC_{50} value in the inhibition of OAT1-mediated ^{14}C-PAH uptake, and lower K_m in the induction of ^{14}C-PAH efflux compared with FAMT (Table 1), the effect of fluorine-to-iodine substitution was examined in the interaction with OAT1. When the halogen group was located at position 2 on the benzene ring (with a 4-hydroxyl group), the halogen group, whether it was iodine or fluorine, had a profound effect on inhibition and efflux (Fig. 6A–B). 2-FT did not inhibit OAT1 at the concentrations tested (Fig. 6A). Consistent with this, the efflux induced by 2-FT was much reduced compared to that induced by 2-IT (Fig. 6B). When the halogen group was at position 3 on the benzene ring (with a 4-hydroxyl group), the impact of iodine or fluorine on the interaction with OAT1 was reduced compared with a halogen at position 2 (Fig. 6C–D). IC_{50} of 3-FT was 3.2-fold higher than that of 3-IT in inhibition experiments, whereas the K_m of 3-FT in the induction of ^{14}C-PAH efflux was 4.6-fold higher than that of 3-IT (Table 1). Finally, when the halogen group was at position 4 (with a 3-hydroxyl group), the IC_{50} and K_m values of 4-F-*m*-Tyr were similar to those of 4-I-*m*Tyr; IC_{50} and K_m of 4-F-*m*-Tyr were 0.72-fold and 0.93-fold of IC_{50} and K_m of 4-I-*m*Tyr, respectively (Fig. 6E–F and Table 1).

JPET Fast Forward. Published on September 27, 2020 as DOI: 10.1124/jpet.120.000235
This article has not been copyedited and formatted. The final version may differ from this version.

Interactions of 2-FAMT with OAT1, and amino acid transporters LAT1 and LAT2

Because 2-FT interacted the least with OAT1 (Fig. 5A), we expected that 2-FAMT, in which an α-methyl group is added to 2-FT to promote LAT1-specificity (Wiriyasermkul et al., 2012; Wei et al., 2016b), might be an LAT1-specific substrate with reduced OAT1 interaction. As shown in Fig. 7A–B, 2-FAMT exhibited decreased inhibition of OAT1-mediated ^{14}C-PAH uptake and induced decreased OAT1-mediated ^{14}C-PAH efflux compared with FAMT.

LAT1-specific transport of 2-FAMT was further confirmed by efflux experiments. 2-FAMT induced LAT1-mediated efflux of preloaded ^{14}C-L-leucine, whereas it did not induce efflux of preloaded ^{14}C-L-alanine mediated by LAT2 which is closely related to LAT1 (Supplemental Fig. 3A–B), indicating that 2-FAMT was transported by LAT1 but not by LAT2. The LAT1-selectivity of 2-FAMT was similar to that of FAMT, whereas 2-FT, lacking an α-methyl group, was transported by both LAT1 and LAT2 (Supplemental Fig. 3A–B).

Renal handling and tumor accumulation: comparison of FAMT, 2-FAMT, and 2-FT in vivo

JPET Fast Forward. Published on September 27, 2020 as DOI: 10.1124/jpet.120.000235
This article has not been copyedited and formatted. The final version may differ from this version.

The involvement of the organic anion transport system in the renal handling of FAMT was examined *in vivo* using probenecid, an inhibitor of organic anion transporters, including OAT1. In ddY mice intravenously administered FAMT, the probenecid treatment reduced the renal accumulation of FAMT by 80% ($p < 0.001$) (Fig. 8A), and reduced urinary excretion of FAMT by 66%, compared with the non-treated control ($p = 0.0012$) (Fig. 8B). The plasma concentration of FAMT was, in contrast, increased by probenecid ($p = 0.0045$). This suggests that FAMT is mainly secreted into the urine via a trans-epithelial organic-anion transport system and that the site of action of probenecid may be on the basolateral side where OAT1 is localized as discussed in detail later.

Because 2-FT and 2-FAMT showed reduced interaction with OAT1 *in vitro* (Fig. 5A–B and Fig. 7), we compared their renal accumulation, urinary excretion, and plasma concentration with those of FAMT *in vivo*. In ddY mice intravenously administered equimolar amounts of FAMT, 2-FAMT, or 2-FT, lower renal accumulation and lower urinary excretion were observed following 2-FAMT or 2-FT administration compared with FAMT administration (Fig. 8D–E). Notably, 2-FAMT showed a relatively higher plasma concentration than FAMT, although the difference was not statistically significant (Fig. 8F). In the pharmacokinetic study conducted in

JPET Fast Forward. Published on September 27, 2020 as DOI: 10.1124/jpet.120.000235
This article has not been copyedited and formatted. The final version may differ from this version.

mice, 2-FAMT exhibited a lower rate constant of elimination from the plasma (K_e), and the longer half-life in the plasma ($t_{1/2}$) compared with FAMT (Table 2). Furthermore, the renal clearance (CL_{renal}) of 2-FAMT was lower than that of FAMT (Table 2).

Due to the low renal accumulation and LAT1-specific transport of 2-FAMT, we examined the tumor accumulation of 2-FAMT and compared with that of FAMT. In tumor-bearing C57BL/6J mice injected intravenously with FAMT or 2-FAMT, the accumulation of 2-FAMT in the tumor was 1.56-fold higher than that of FAMT after 1 h (p = 0.0192) (Fig. 8G). The renal accumulation of 2-FAMT was 0.53-fold of that of FAMT after 1 h (p = 0.0142). At 10 min after administration, no difference was detected between 2-FAMT and FAMT in tumor or in the kidney. Neither was any difference observed between FAMT and 2-FAMT accumulation in the skeletal muscle after 10 min or 1 h. FAMT and 2-FAMT did not exhibit differences in the tumor-to-plasma concentration ratio of free compounds at 1 h estimated based on the protein-unbound free compound fraction (f_u) obtained *in vitro* (Fig. 8H).

JPET Fast Forward. Published on September 27, 2020 as DOI: 10.1124/jpet.120.000235
This article has not been copyedited and formatted. The final version may differ from this version.

Discussion

In the present study, we demonstrated that FAMT is transported by renal organic anion transporter OAT1 concentration-dependently (Fig. 2). To optimize the halogenated compounds that exhibit low interaction with OAT1 and high specificity for LAT1-mediated transport, we investigated the structural requirements of FAMT for interaction with OAT1. On the basis of previous reports showing remarkably decreased renal accumulation of 4-I-*m*-Tyr compared with IMT, which is structurally identical to FAMT except for a fluorine/iodine substitution (Shikano et al., 2003), we found that 4-I-*m*-Tyr interacted less with OAT1 than IMT did, in both inhibition and efflux studies (Fig. 3). In comparing distinct structures, the 3-halogen and 4-hydroxyl groups of IMT and FAMT were essential for interaction with OAT1, whereas the α-methyl group contributed to a lesser extent but it was still relevant (Fig. 4 and Table 1).

It has been proposed that the preferred substrates of PAH transporter at the basolateral membrane of renal proximal tubules, where OAT1 is located, contain hydrophobic cores with negative ionic or partial charges (Ullrich and Rumrich,1988). These requirements were confirmed for OAT1 (Apiwattanakul et al.,1999). The binding of organic anions would, thus, depend on both hydrophobic and electrostatic interactions (Moller and Sheikh, 1982; Fritzsch et al., 1989). Because the presence of the α-methyl

JPET Fast Forward. Published on September 27, 2020 as DOI: 10.1124/jpet.120.000235
This article has not been copyedited and formatted. The final version may differ from this version.

group decreased IC_{50} values for both IMT and FAMT (Table 1), the α-methyl group was hypothesized to be involved in the makeup of the hydrophobic core. The *ortho*-position of the benzene ring, close to the α-methyl group, may also be located in the central part of the hydrophobic core, because the substitution of fluorine with a bulky, hydrophobic iodine atom at the *ortho*-position dramatically increased the interaction with OAT1 (Fig. 6A–B). This influence is reduced at the *meta*-position (Fig. 6C–D), and almost negligible at the *para*-position (Fig. 6E–F). The *para*-position would, thus, represent the margin of the effective hydrophobic core. This hypothesis is consistent with the preferred size of hydrophobic core, which has been proposed to be 6–10 Å in the renal PAH transport (Fritzsch et al., 1989), because the distance from the carbonyl carbon of the α-carboxyl group to the fluoro/iodo group at the *ortho*-, *meta*- and *para*-positions are estimated to be 4.45/4.62, 6.92/7.52 and 7.94/8.69 Å, respectively (Supplemental Fig. 4).

As negative ionic or partial charges are required for substrate binding (Ullrich and Rumrich,1988), the α-carboxyl group is considered to have a negative ionic charge. Furthermore, the hydroxyl group on benzene ring, necessary for interaction with OAT1, may behave as an additional negative partial charge, because the pK_a of a phenolic hydroxyl group is inversely related to the interaction with the PAH transporter (Fritzsch et al., 1989). The present study confirmed the tendency of an inverse relationship between

JPET Fast Forward. Published on September 27, 2020 as DOI: 10.1124/jpet.120.000235
This article has not been copyedited and formatted. The final version may differ from this version.

the inhibitory activity of the compound and the estimated pK_a of the hydroxyl group on the benzene ring (Supplemental Fig. 5). The role of the halogen group, which is also necessary, is further proposed to stabilize or increase the negative partial charge of the hydroxyl group, due to the electron-attraction which lowers the pK_a of the hydroxyl group on the benzene ring. In the absence of the halogen group, the negative partial charge of the hydroxyl group would not be enough to interact with OAT1 (Table 1).

Intriguingly, the hydroxyl group may be localized at any position on the benzene ring and still maintain interaction with OAT1 (Fig. 5). Due to the mutual structural adjustments of substrates and the binding site, the hydroxyl group, whether it is at *ortho*-, *meta*-, or *para*-positions, may be located to the negative charge recognition site, whereas the α-carboxyl group is placed at the other negative charge recognition site (Supplemental Fig. 6A–C). The hydrophobic core involving a fluorine at any position may be accepted by the hydrophobic pocket in the binding site (Fritzsch et al., 1989) when the hydroxyl group is at the *ortho*-position (Fig. 5E–F and Supplemental Fig. 6A). By contrast, the distance between the hydrophobic core of the substrate and the bottom of the hydrophobic pocket would be increased when the hydroxyl group is at the *meta*- or *para*-position (Supplemental Fig. 6B–C). The vacant space formed between the hydrophobic core and the hydrophobic pocket may be more prominent when fluorine is at the *ortho*-position

JPET Fast Forward. Published on September 27, 2020 as DOI: 10.1124/jpet.120.000235
This article has not been copyedited and formatted. The final version may differ from this version.

(Supplemental Fig. 6B–C), because 2-FT and 6-F-*m*-Tyr showed reduced interaction (Fig. 5). This vacant space could be filled with the bulkier iodine, because the replacement of fluorine with iodine at the *ortho*-position dramatically increased the interaction (Fig. 6A–B).

As a candidate of halogenated compound with low interaction with OAT1 and high LAT1-specificity, we examined 2-FAMT in which the α-methyl group, that provides LAT1-specificity (Wiriyasermkul et al., 2012; Wei et al., 2016b), is added to 2-FT which demonstrated the least interaction with OAT1. LAT1-selective transport of 2-FAMT was confirmed, in comparison with FAMT and 2-FT (Supplemental Fig. 3). As expected, 2-FAMT exhibited less interaction with OAT1 compared with FAMT (Fig. 7 and Supplemental Fig. 7).

In *in vivo* experiments that address the renal handling, both renal accumulation and urinary excretion of FAMT were suppressed by probenecid, whereas the plasma concentration was increased (Fig. 8A–C), suggesting that FAMT is excreted into urine mainly via trans-epithelial transport in the basolateral-to-apical direction. This observation is consistent with previous studies showing that renal accumulation and urinary excretion of IMT were decreased by probenecid (Shikano et al., 2004b; Nakajima et al., 2007). Trans-epithelial organic anion excretion is an accumulative process in which intracellular

JPET Fast Forward. Published on September 27, 2020 as DOI: 10.1124/jpet.120.000235
This article has not been copyedited and formatted. The final version may differ from this version.

concentration of organic anions can rise to 100–300 times the concentration in the peritubular fluid, because organic anion transporters, including OAT1 involved in this process mediate tertiary active transport (Shikano et al., 2004a; Schäli and Roch-Ramel, 1980); this may account for the renal accumulation of FAMT in the course of trans-epithelial transport.

The effects of probenecid on the renal accumulation, urinary excretion and plasma concentration of FAMT suggest that the primary site of action of probenecid is the basolateral side of the proximal tubules, although probenecid blocks organic anion transporters involved in uptake and efflux on both the apical and basolateral membrane of proximal tubules (Pelis and Wright, 2011; Brazeau, 1975). We previously showed that, among organic ion transporters mediating uptake into tubular epithelial cells, OAT1, OAT10, and OCTN2 transported FAMT, whereas OAT3, OAT4, URAT1, OCTN1, OCT1, and OCT2 did not transport FAMT (Wei et al., 2016a). Reduced transport of FAMT by OAT3 was confirmed in the present study, along with 2-FAMT and 2-FT (Supplemental Fig. 7). Because OAT3 preferentially transports compounds with larger molecular size and larger nonpolar surface area compared with OAT1, FAMT-related compounds may not be preferable substrates of OAT3 (Astorga et al., 2011). Although OAT2, mainly expressed in the liver in humans, was not examined in our study, the contribution of OAT2 to FAMT

JPET Fast Forward. Published on September 27, 2020 as DOI: 10.1124/jpet.120.000235
This article has not been copyedited and formatted. The final version may differ from this version.

transport may be less plausible, due to the negligible liver accumulation of FAMT observed via ^{18}F-FAMT-PET imaging (Vildhede et al., 2018; Inoue et al., 2001; Hanaoka et al., 2019). Among OAT1, OAT10, and OCTN2, the basolateral membrane transporter OAT1 is involved in the trans-epithelial accumulative organic anion excretion in the basolateral-to-apical direction (Anzai et al., 2006). Therefore, OAT1 is supposed to be the most important transporter responsible for the high renal background of tumor-specific amino acid tracers such as ^{18}F-FAMT and ^{123}I-IMT.

Consistent with the proposed role of OAT1 in the renal handling of FAMT and related compounds, 2-FAMT and 2-FT showed reduced interaction with OAT1 (Fig. 5 and 7) and exhibited less renal accumulation and urinary excretion compared with FAMT (Fig. 8D–E). In the pharmacokinetic study, we confirmed that the renal clearance (CL_{renal}) of 2-FAMT was lower than that of FAMT (Table 2). As indicated above, 2-FAMT is LAT1-selective, whereas 2-FT is not (Supplemental Fig. 3). Therefore, we examined the tumor accumulation of 2-FAMT in tumor-bearing mice and found that 2-FAMT exhibited higher tumor uptake with less renal accumulation compared with FAMT (Fig. 8G). Because the tumor-to-plasma ratio 2-FAMT was not different from that of FAMT (Fig. 8H), the higher tumor accumulation of 2-FAMT would be due to the higher plasma exposure compared with FAMT (Table 2 and Fig. 8F). Increased tumor uptake upon

JPET Fast Forward. Published on September 27, 2020 as DOI: 10.1124/jpet.120.000235
This article has not been copyedited and formatted. The final version may differ from this version.

inhibition of renal accumulation and urinary excretion was also demonstrated by IMT (Nakajima et al., 2007). Additionally, 2-fluoro-α-methyl-L-phenylalanine, lacking a ring-hydroxyl group and so presumably less interactive with OAT1, has been shown to have higher tumor uptake and lower renal accumulation than FAMT (Hanaoka et al., 2019). These observations suggest that reducing the interaction with OAT1 may be beneficial to improve tumor targeting as well as to suppress renal accumulation. Such a strategy could also be useful for targeted alpha therapy. In this respect, ^{211}At-labeled α-methyl phenylalanine would be a preferable candidate for cancer-specific targeted alpha therapy that causes less renal damage. The α-methyl tyrosine with *ortho*-^{211}At should be avoided because the bulky ^{211}At atom would likely increase the interaction with OAT1 (Fig. 6). The present study would also support the use of *para*-^{211}At-phenylalanine (Watabe et al., 2020), which exhibited remarkable anti-tumor effects in mice with less obvious toxicity.

JPET Fast Forward. Published on September 27, 2020 as DOI: 10.1124/jpet.120.000235
This article has not been copyedited and formatted. The final version may differ from this version.

Authorship Contributions

Participated in research design: Kanai, Jin, Nagamori, Ohgaki, Okuda, Okanishi, He

Conducted experiments: Jin, Wei, Ohgaki, Tominaga, Xu, Kawamoto

Performed data analysis: Jin, Wei, Kanai

Wrote or contributed to the writing of the manuscript: Jin, Kanai

JPET Fast Forward. Published on September 27, 2020 as DOI: 10.1124/jpet.120.000235
This article has not been copyedited and formatted. The final version may differ from this version.

References

Anzai N, Kanai Y, and Endou H (2006) Organic anion transporter family: current knowledge. *J Pharmacol Sci.* **100**:411-426.

Apiwattanakul N, Sekine T, Chairoungdua A, Kanai Y, Nakajima N, Sophasan S, and Endou H (1999) Transport properties of nonsteroidal anti-inflammatory drugs by organic anion transporter 1 expressed in *Xenopus laevis* oocytes. *Mol Pharmacol.* **55**:847-854.

Astorga B, Wunz TM, Morales M, Wright SH, and Pelis RM (2011) Differences in the substrate binding regions of renal organic anion transporters 1 (OAT1) and 3 (OAT3). *Am J Physiol Renal Physiol.* **301**:378-386.

Brazeau P. (1975) Inhibitors of tubular transport of organic compounds, in *The Pharmacologic basis of Therapeutics* (Goodman L and Gliman A eds) pp 862-863, MacMillan Publishing Co., Inc., New York

Cook GJ, Maisey MN, and Fogelman I (1999) Normal variants, artefacts and interpretative pitfalls in PET imaging with 18-fluoro-2-deoxyglucose and carbon-11 methionine. *Eur J Nucl Med.* **10**:1363-1378.

Fritzsch G, Rumrich G, and Ullrich KJ (1989) Anion transport through the contraluminal cell membrane of renal proximal tubule. The influence of hydrophobicity and molecular charge distribution on the inhibitory activity of organic anions. *Biochim*

Biophys Acta. **978**:249-256.

Hanaoka H, Ohshima Y, Yamaguchi A, Suzuki H, Ishioka NS, Higuchi T, Arano Y, and Tsushima Y (2019) Novel ^{18}F-Labeled α-Methyl-Phenylalanine Derivative with High Tumor Accumulation and Ideal Pharmacokinetics for Tumor-Specific Imaging. *Mol Pharm.* **16**:3609-3616.

Ichida K, Hosoyamada M, Kimura H, and Takeda M (2003) Urate transport via human PAH transporter hOAT1 and its gene structure. *Kidney Int.* **63**:143-155.

Imaoka T, Kusuhara H, Adachi M, Schuetz JD, Takeuchi K, and Sugiyama Y (2007) Functional involvement of multidrug resistance-associated protein 4 (MRP4/ABCC4) in the renal elimination of the antiviral drugs adefovir and tenofovir. *Mol Pharmacol.* **71**:619-27.

Inoue T, Koyama K, Oriuchi N, Alyafei S, Yuan Z, Suzuki H, Takeuchi K, Tomaru Y, Tomiyoshi K, Aoki J, and Endo K (2001) Detection of malignant tumors: whole-body PET with fluorine 18 alpha-methyl tyrosine versus FDG--preliminary study. *Radiology.* **220**:54-62.

Jager PL, Vaalburg W, Pruim J, de Vries EG, Langen KJ, and Piers DA (2001) Radiolabeled amino acids: basic aspects and clinical applications in oncology. *J Nucl Med* **42**:432–445.

Kanai Y, Segawa H, Miyamoto Ki, Uchino H, Takeda E, and Endou H (1998) Expression cloning and characterization of a transporter for large neutral amino acids activated by the heavy chain of 4F2 antigen (CD98). *J Biol Chem.* **274**:23629-23632.

Kandasamy P, Gyimesi G, Kanai Y, and Hediger MA (2018) Amino acid transporters revisited: New views in health and disease. *Trends Biochem Sci.* **43**:752–789.

Møller JV and Sheikh MI (1982) Renal organic anion transport system: pharmacological, physiological, and biochemical aspects. *Pharmacol Rev.* **34**:315-358.

Nagamori S, Wiriyasermkul P, Guarch ME, Okuyama H, Nakagomi S, Tadagaki K, Nishinaka Y, Bodoy S, Takafuji K, Okuda S, Kurokawa J, Ohgaki R, Nunes V, Palacín M, and Kanai Y (2016) Novel cystine transporter in renal proximal tubule identified as a missing partner of cystinuria-related plasma membrane protein rBAT/SLC3A1. *Proc Natl Acad Sci U S A.* **113**:775-780.

Nakajima S, Shikano N, Kotani T, Ogura M, Nishii R, Yoshimoto M, Yamaguchi N, Iwamura Y, Kubota N, Ishikawa N, and Kawai K (2007) Pharmacokinetics of 3-[^{125}I]iodo-alpha-methyl-L-tyrosine, a tumor imaging agent, after probenecid loading in mice implanted with colon cancer DLD-1 cells. *Nucl Med Biol.* **34**:1003-1008.

Ohgaki R, Wei L, Yamada K, Hara T, Kuriyama C, Okuda S, Ueta K, Shiotani M, Nagamori S, and Kanai Y (2016) Interaction of the Sodium/Glucose Cotransporter (SGLT)

2 inhibitor Canagliflozin with SGLT1 and SGLT2. *J Pharmacol Exp Ther.* **358**:94-102.

Ohshima Y, Hanaoka H, Tominaga H, Kanai Y, Kaira K, Yamaguchi A, Nagamori S, Oriuchi N, Tsushima Y, Endo K and Ishioka NS. (2013) Biological evaluation of 3-[$^{(18)}$F]fluoro-α-methyl-D-tyrosine (D-[$^{(18)}$F]FAMT) as a novel amino acid tracer for positron emission tomography. *Ann Nucl Med.* **27**:314-24.

Pelis RM and Wright SH (2011) Renal transport of organic anions and cations. *Compr Physiol.* **1**:1795-835.

Plathow C and Weber WA (2008) Tumor cell metabolism imaging. *J Nucl Med.* **49**: 43S-63S.

Schäli C and Roch-Ramel F (1980) Accumulation of [^{14}C]urate and [^{3}H]PAH in isolated proximal tubular segments of the rabbit kidney. *Am J Physiol.* **239**:222-227.

Sekine T, Watanabe N, Hosoyamada M, Kanai Y, and Endou H (1997) Expression cloning and characterization of a novel multispecific organic anion transporter. *J Biol Chem.* **272**:18526-18529.

Shikano N, Kawai K, Flores LG 2nd, Nishii R, Kubota N, Ishikawa N, and Kubodera A (2003) An artificial amino acid, 4-iodo-L-meta-tyrosine: biodistribution and excretion via kidney. *J Nucl Med.* **44**:625-631.

Shikano N, Kanai Y, Kawai K, Ishikawa N, and Endou H (2004a) Transport of

99mTc-MAG3 via rat renal organic anion transporter 1. *J Nucl Med.* **45**:80-85.

Shikano N, Kawai K, Nakajima S, Nishii R, Flores LG 2nd, Kubodera A, Kubota N, Ishikawa N, and Saji H (2004b) Renal accumulation and excretion of radioiodinated 3-iodo-α-methyl-L- tyrosine. *Ann Nucl Med* **18**:263-270

Shiraya K, Hirata T, Hatano R, Nagamori S, Wiriyasermkul P, Jutabha P, Matsubara M, Muto S, Tanaka H, Asano S, Anzai N, Endou H, Yamada A, Sakurai H, and Kanai Y (2010) A novel transporter of SLC22 family specifically transports prostaglandins and co-localizes with 15-hydroxyprostaglandin dehydrogenase in renal proximal tubules. *J Biol Chem.* **285**:22141-22151.

Suzuki S, Kaira K, Ohshima Y, Ishioka NS, Sohda M, Yokobori T, Miyazaki T, Oriuchi N, Tominaga H, Kanai Y, Tsukamoto N, Asao T, Tsushima Y, Higuchi T, Oyama T, and Kuwano H (2014) Biological significance of fluorine-18-α-methyltyrosine (FAMT) uptake on PET in patients with oesophageal cancer. *Br J Cancer.* **110**:1985-1991.

Uchino H, Kanai Y, Kim DK, Wempe MF, Chairoungdua A, Morimoto E, Anders MW, and Endou H (2002) Transport of amino acid-related compounds mediated by L-type amino acid transporter 1 (LAT1): insights into the mechanisms of substrate recognition. *Mol Pharmacol.* **61**:729-737.

Ullrich KJ and Rumrich G (1988) Contraluminal transport systems in the proximal

renal tubule involved in secretion of organic anions. *Am J Physiol.* **254**:453-462.

Vildhede A, Kimoto E, Rodrigues AD and Varma MVS (2018) Quantification of Hepatic Organic Anion Transport Proteins OAT2 and OAT7 in Human Liver Tissue and Primary Hepatocytes. *Mol Pharm.* **15**:3227-3235.

Watabe T, Kaneda-Nakashima K, Shirakami Y, Liu Y, Ooe K, Teramoto T, Toyoshima A, Shimosegawa E, Nakano T, Kanai Y, Shinohara A and Hatazawa J (2020) Targeted alpha therapy using astatine (^{211}At)-labeled phenylalanine: A preclinical study in glioma bearing mice. *Oncotarget.* **11**:1388-1398.

Wei L, Tominaga H, Ohgaki R, Wiriyasermkul P, Hagiwara K, Okuda S, Kaira K, Kato Y, Oriuchi N, Nagamori S, and Kanai Y. (2016a) Transport of 3-fluoro-L-α-methyl-tyrosine (FAMT) by organic ion transporters explains renal background in [(^{18})F]FAMT positron emission tomography. *J Pharmacol Sci.* **130**:101-109.

Wei L, Tominaga H, Ohgaki R, Wiriyasermkul P, Hagiwara K, Okuda S, Kaira K, Oriuchi N, Nagamori S, and Kanai Y (2016b) Specific transport of 3-fluoro-l-α-methyl-tyrosine by LAT1 explains its specificity to malignant tumors in imaging. *Cancer Sci.* **107**:347-352.

Wiriyasermkul P, Nagamori S, Tominaga H, Oriuchi N, Kaira K, Nakao H, Kitashoji

T, Ohgaki R, Tanaka H, Endou H, Endo K, Sakurai H, and Kanai Y (2012) Transport of 3-fluoro-l-α-methyl-tyrosine by tumor-upregulated L-type amino acid transporter 1: a cause of the tumor uptake in PET. *J Nucl Med*. **53**:1253-1261

Wongthai P, Hagiwara K, Miyoshi Y, Wiriyasermkul P, Wei L, Ohgaki R, Kato I, Hamase K, Nagamori S, and Kanai Y (2015) Boronophenylalanine, a boron delivery agent for boron neutron capture therapy, is transported by $ATB^{0,+}$, LAT1 and LAT2. *Cancer Sci.* **106**:279-286.

JPET Fast Forward. Published on September 27, 2020 as DOI: 10.1124/jpet.120.000235
This article has not been copyedited and formatted. The final version may differ from this version.

Footnotes

This work was supported by Grants-in-Aid for Scientific Research from the Japan Society for the Promotion of Science (to Y.K. 19H03407); the Project for Development of Innovative Research on Cancer Therapeutics from Japan Agency for Medical Research and Development (to Y.K. 17cm0106118, JP18cm0106131, JP19cm0106151, and JP20cm0106151).

This work was previously presented in part as follows: *the 18th World congress of basic and clinical pharmacology,* July, 2, 2018, Kyoto, Japan; *The 92nd Annual Meeting for the Japanese Pharmacological Society*, March, 14, 2019, Osaka, Japan

[1] Present address is: Department of Internal medicine, Osaka Police Hospital, 10-31 Kitayamacho, Osaka Tennoji-ku, Osaka 543-0035, Japan

JPET Fast Forward. Published on September 27, 2020 as DOI: 10.1124/jpet.120.000235
This article has not been copyedited and formatted. The final version may differ from this version.

Figure legends

Figure 1. Chemical structures of compounds used in this study.

(*A*) α-Methyl aromatic amino acids. **(*B*)** Iodinated aromatic amino acids. **(*C*)**Fluorinated aromatic amino acids. Groups I, II, and III represent compounds with hydroxyl group at the *para*, *meta*, and *ortho* positions of the benzene ring, respectively.

Figure 2. Transport of FAMT by OAT1.

(*A*) Concentration-dependent inhibition of ^{14}C-PAH uptake by FAMT in OAT1 cells. Uptake of ^{14}C-PAH (1μM) was measured in the presence of various concentrations of FAMT. Uptake values were fitted to inhibition curves. IC_{50} of FAMT on OAT1-mediated ^{14}C-PAH uptake was 453.1 ± 14.3 μM (n = 4). **(*B*)** Concentration dependence of FAMT-induced ^{14}C-PAH efflux in OAT1 cells. The efflux of preloaded ^{14}C-PAH from OAT1 cells was measured for 1 min in the presence or absence of extracellular FAMT. The FAMT-induced efflux at each concentration of FAMT was obtained as described in "Materials and Methods" and plotted against the concentration of FAMT. The curve fit to Michaelis–Menten equation. The inset shows Eadie–Hofstee plot (ordinate: V (% radioactivity/min); abscissa: V (% radioactivity/min)/[FAMT] (μM)), which was used to determine kinetic parameters. K_m of 690.8 ± 18.9 μM and V_{max} of 38.1± 7.3%

JPET Fast Forward. Published on September 27, 2020 as DOI: 10.1124/jpet.120.000235
This article has not been copyedited and formatted. The final version may differ from this version.

radioactivity/min were obtained (n = 4). **(*C*)** Concentration dependence of ^{14}C-FAMT uptake mediated by OAT1. OAT1-mediated uptake of ^{14}C-FAMT at each concentration was measured for 1 min. Uptake rates were fit to Michaelis-Menten curve. Inset shows Eadie-Hofstee plot (ordinate: V (pmol/mg protein/min); abscissa: V (pmol/mg protein/min)/[FAMT] (μM)). K_m of 171.9 ± 16.6 μM and V_{max} of 3,391 ± 27.3 pmol/mg/min were obtained (n = 4).

Figure 3. Comparison of IMT and 4-I-*m*-Tyr in interaction with OAT1

(*A*) Concentration-dependent inhibition of ^{14}C-PAH uptake by IMT and 4-I-*m*-Tyr in OAT1 cells. Uptake of ^{14}C-PAH (1μM) was measured in the presence of varied concentrations of IMT or 4-I-*m*-Tyr. Uptake values were fitted to inhibition curves with IC_{50} listed in Table 1. **(*B*)** ^{14}C-PAH efflux mediated by OAT1 induced by IMT and 4-I-*m*-Tyr. The efflux of preloaded ^{14}C-PAH from OAT1 cells was measured for 1 min in the presence or absence (−) of extracellular compounds at the indicated concentration. The radioactivity released from the cells was expressed as the percent of total preloaded radioactivity. * $p < 0.05$; ** $p < 0.01$; *** $p < 0.001$ vs. (−). Data are expressed as means ± SD (n = 4).

JPET Fast Forward. Published on September 27, 2020 as DOI: 10.1124/jpet.120.000235
This article has not been copyedited and formatted. The final version may differ from this version.

Figure 4. Effect of removal of α-methyl-, hydroxyl- or halogen group from IMT and FAMT

The concentration-dependent inhibition of ^{14}C-PAH uptake (***A***) and the induction of OAT1-mediated ^{14}C-PAH efflux (***B***) were compared among IMT and the compounds (3-IT, 3-I-AMP, and AMT) in which α-methyl-, hydroxyl- or halogen group was removed from IMT. The effect of removal of α-methyl-, hydroxyl- and halogen groups was also examined for FAMT in the comparison with 3-FT, 3-F-AMP, and AMT: the inhibition of ^{14}C-PAH uptake (***C***); the induction of ^{14}C-PAH efflux (***D***). The inhibition and efflux experiments were performed as described in the legend to **Fig. 3**. Uptake values were fitted to inhibition curves except 3-F-AMP and 3-I-AMP that were difficult to fit (***A*** and ***C***). AMT in ***C*** same as that in ***A*** is shown as comparison. In ***B*** and ***D***, * $p < 0.05$; ** $p < 0.01$; *** $p < 0.001$ vs. (−). Data are expressed as means ± SD (n = 4).

Figure 5. Effect of fluoro-group position in *para*-tyrosine, *meta*-tyrosine and *ortho*-tyrosine

The effect of fluoro-group position was examined with a hydroxyl group fixed at position 4 (*para*-position), position 3 (*meta*-position) or position 2 (*ortho*-position) of benzene ring. The concentration-dependent inhibition of ^{14}C-PAH uptake (***A, C*** and ***E***) and the induction

JPET Fast Forward. Published on September 27, 2020 as DOI: 10.1124/jpet.120.000235
This article has not been copyedited and formatted. The final version may differ from this version.

of OAT1-mediated ^{14}C-PAH efflux (***B, D*** and ***F***) were compared between the compounds at indicated concentrations. The inhibition and efflux experiments were performed as described in the legend to Fig. 3. In ***A***, ***C*** and ***E***, the uptake values were fitted to inhibition curves except 2-FT that was difficult to fit. 3-FT in ***A*** same as that in Fig. 4C is shown as comparison. In ***B, D*** and ***F***, * $p < 0.05$; ** $p < 0.01$; *** $p < 0.001$ vs. (-). Data are expressed as means ± SD (n = 4).

Figure 6. Comparison of fluoro and iodo groups in the interaction with OAT1

The contribution of fluoro and iodo groups in the interaction with OAT1 was compared between the compound with fluoro group and that with iodo group at the same position: 2-FT and 2-IT (***A***); 3-FT and 3-IT (***B***); 4-F-*m*-Tyr and 4-I-*m*-Tyr (***A***). The inhibition of ^{14}C-PAH uptake (***A***, ***C*** and ***E***) and the induction of OAT1-mediated ^{14}C-PAH efflux (***B***, ***D*** and ***F***) were examined as described in the legend to Fig. 3. In ***A***, ***C*** and ***E***, the uptake values were fitted to inhibition curves, whereas the efflux values are fitted to *Michaelis–Menten* curves in ***B***, ***D*** and ***F***. Blue: compounds with a fluoro group; black: and compounds with an iodo group. In ***A***, ***C*** and ***E***, the compounds except 2-IT were presented in the other figures and shown for comparison (2-FT from Fig. 5; 3-FT and 3-IT from Fig. 5; 4-F-*m*-Tyr from Fig. 6; 4-I-*m*-Tyr from Fig. 3). Data represent means ± SD, n = 4.

JPET Fast Forward. Published on September 27, 2020 as DOI: 10.1124/jpet.120.000235
This article has not been copyedited and formatted. The final version may differ from this version.

Figure 7. Interaction of 2-FAMT with OAT1.

2-FAMT that has a fluoro group at position 2 and FAMT with a fluoro group at position 3 were compared in the inhibition of ^{14}C-PAH uptake (***A***) and the induction of OAT1-mediated ^{14}C-PAH efflux (***B***). 2-FAMT exhibited less inhibition on OAT1-mediated ^{14}C-PAH uptake than FAMT (***A***). Similarly, 2-FAMT induced less ^{14}C-PAH efflux mediated by OAT1 compared with FAMT (***B***). The inhibition and efflux experiments were performed as described in the legend to Fig. 3. FAMT in ***A*** same as that in Fig. 4C is shown as comparison. In ***B***, * $p < 0.05$; ** $p < 0.01$; *** $p < 0.001$ vs. (-). Data are expressed as means ± SD (n = 4).

Figure 8. *In vivo* studies of FAMT, 2-FAMT and 2-FT on their renal handling and tumor accumulation.

(*A, B, C*) The effect of probenecid on renal handling of FAMT in mice. The renal accumulation, urinary excretion and plasma concentration of FAMT at 10 min after the intravenous administration of FAMT (1.5 mg/kg) were measured with and without probenecid treatment in ddY mice. Probenecid (50 mg/kg) was pre-administered intravenously 10 min before the injection of FAMT. Treatment with probenecid reduced

JPET Fast Forward. Published on September 27, 2020 as DOI: 10.1124/jpet.120.000235
This article has not been copyedited and formatted. The final version may differ from this version.

renal accumulation **(*A*)**, decreased urinary excretion **(*B*)** and increased plasma concentration **(*C*)** of FAMT. **(*D, E, F*)** Comparison of FAMT, 2-FAMT and 2-FT administered in mice. Renal accumulation, urinary excretion and plasma concentration were measured at 10 min after the intravenous administration of equimolar amounts of FAMT (1.5 mg/kg), 2-FAMT (1.5 mg/kg) and 2-FT (1.4 mg/kg) in ddY mice. The renal accumulation **(*D*)** and urinary excretion **(*E*)** of 2-FAMT and 2-FT were lower than those of FAMT. (***G***) Comparison of 2-FAMT and FAMT in tumor accumulation. The accumulation of 2-FAMT and FAMT in tumor as well as kidney and skeletal muscle was measured at 10 min and 1 hour after the intravenous administration in B16F10 tumor-bearing mice. At 1 hour, 2-FAMT showed 1.56 times higher accumulation compared with FAMT in the tumor, whereas the renal accumulation of 2-FAMT was 0.53 times lower than that of FAMT. At 10 min, no significant differences were detected between 2-FAMT and FAMT in tumor as well as in kidney. In the skeletal muscle, no difference was observed either at 10 min or 1 hour. Results are expressed as percentage of injected dose normalized per gram tissue and per mL plasma for kidney and plasma, respectively. Urinary excretion is expressed as percentage of injected dose for whole collected urine. (***H***) Comparison of tumor-to-plasma concentration ratio of free compounds between FAMT and 2-FAMT in B16F10 tumor-bearing mice at 1 h after the

JPET Fast Forward. Published on September 27, 2020 as DOI: 10.1124/jpet.120.000235
This article has not been copyedited and formatted. The final version may differ from this version.

intravenous administration. The tumor-to-plasma concentration ratio was determined by dividing the estimated amount of free compound in the tumor (normalized to per gram of tumor tissue) by that in the plasma (normalized to per milliliter of plasma). The protein-unbound free compound fractions (f_u) of FAMT and 2-FAMT in plasma were 92.37 ± 7.35% and 90.68 ± 7.29%, respectively. The f_u in tumor homogenate was 90.21 ± 4.68% for FAMT and 89.87 ± 9.61% for 2-FAMT. The concentration of free compound was calculated as the total plasma or tumor tissue concentration times f_u. The tumor-to-plasma concentration ratios of free compounds were comparable between FAMT and 2-FAMT. Data are expressed as means ± SD (n = 4–6). N.S., no statistically significant difference between FAMT and 2-FAMT.

JPET Fast Forward. Published on September 27, 2020 as DOI: 10.1124/jpet.120.000235
This article has not been copyedited and formatted. The final version may differ from this version.

Table.1 Kinetic parameters of each compound on OAT1

Compound	IC_{50} [a] (μM)	K_m of efflux [a] (μM)	estimated pK_a of hydroxyl group [b]
FAMT [c]	453.1 ± 14.3 [d]	690.8 ± 18.9 [d]	8.4
IMT	118.5 ± 12.7	146.8 ± 11.3	8.4
4-I-*m*-Tyr	737.5 ± 12.1	452.7 ± 10.1	8.3
3-IT	236.2 ± 12.7	73.8 ± 6.8	8.3
3-FT	757.1 ± 16.4	339.4 ± 13.4	8.4
3-I-AMP	N.D. [e]		
3-F-AMP	N.D.		
AMT	N.D.		9.3
2-FAMT	N.D.		8.5
2-IT	82.3 ± 15.6	64.0 ± 6.4	8.8
2-FT	N.D.	1166 ± 18.3	8.8
2-F-*m*-Tyr	749.4 ± 24.6		8.3
4-F-*m*-Tyr	534.6 ± 10.3	419.4 ± 19.7	8.3
5-F-*m*-Tyr	371.5 ± 7.2		8.4
6-F-*m*-Tyr	N.D.		8.9

JPET Fast Forward. Published on September 27, 2020 as DOI: 10.1124/jpet.120.000235
This article has not been copyedited and formatted. The final version may differ from this version.

3-F-*o*-Tyr	401.3 ± 9.1	8.2
4-F-*o*-Tyr	607.8 ± 11.4	8.3
5-F-*o*-Tyr	852.5 ± 13.4	8.7
6-F-*o*-Tyr	756.5 ± 19.6	8.3

a) IC_{50} of the compound to inhibit OAT1-mediated ^{14}C-PAH (1μM) uptake and the K_m to induce OAT1-mediated ^{14}C-PAH efflux were determined in OAT1 cells as described in "Materials and Methods".

b) The pK_a value of hydroxyl group on the benzene ring was estimated by the Calculator Plugins, MarvinSketch ver. 20.14.0 (ChemAxon).

c) Kinetic parameters of OAT1-mediated ^{14}C-FAMT uptake were further determined: K_m, 171.9 ± 16.6 μM; V_{max}, 3,391 ± 27.3 pmol/mg/min.

d) Values represent mean ± SD (n = 4)

e) N.D. indicates "not determined".

JPET Fast Forward. Published on September 27, 2020 as DOI: 10.1124/jpet.120.000235
This article has not been copyedited and formatted. The final version may differ from this version.

Table. 2 Pharmacokinetic parameters of FAMT and 2-FAMT in ddY mice

Pharmacokinetic parameters	FAMT	2-FAMT	*p* value [a]
$AUC_{0-\infty}$ (h·μM) [b]	49.23 ± 8.42 [c]	60.24 ± 12.15	0.0806
K_e (h^{-1}) [d]	1.07 ± 0.13	0.86 ± 0.10	0.0131
$t_{1/2}$ (h) [e]	0.65 ± 0.08	0.81 ± 0.11	0.0131
$Ae_{0-\infty}$ (nmol) [f]	114.52 ± 7.73	106.4 ± 13.48	0.0487
CL_{renal} (L/h/kg) [g]	2.39 ± 0.86	1.85 ± 0.38	0.0413

a) FAMT vs. 2-FAMT.

b) $AUC_{0-\infty}$, area under the plasma concentration-time curve from time zero to infinity.

c) Values represent means ± SD (n = 4 to 6).

d) The elimination rate constant (K_e) of FAMT and 2-FAMT was determined following the formula: $\ln C_t = \ln C_0 - K_e \times t$ (C_t: concentration at time t, C_0: initial concentration).

e) $t_{1/2}$, elimination half-life, $t_{1/2} = \ln 2 / K_e$.

f) $Ae_{0-\infty}$, total amount of compounds excreted into urine.

g) The renal clearance (CL_{renal}) of FAMT and 2-FAMT was obtained by dividing $Ae_{0-\infty}$ by $AUC_{0-\infty}$.

A

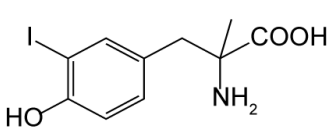

3-iodo-L-α-methyl-tyrosine
(IMT)

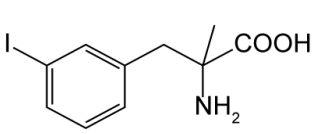

(S)-α-methyl-3-iodophenylalanine
(3-I-AMP)

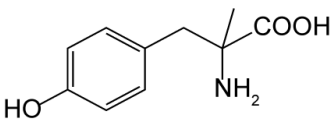

L-α-methyl-tyrosine
(AMT)

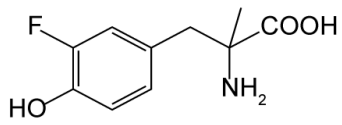

3-fluoro-L-α-methyl-tyrosine
(FAMT)

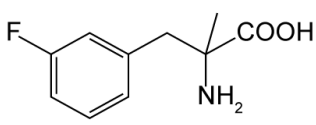

(S)-α-methyl-3-fluorophenylalanine
(3-F-AMP)

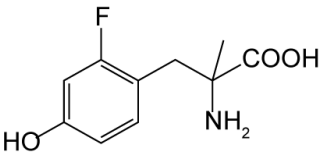

2-fluoro-L-α-methyl-tyrosine
(2-FAMT)

B

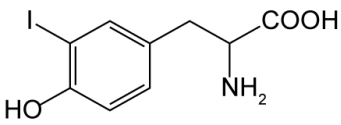

3-iodo-L-tyrosine
(3-IT)

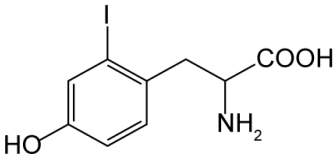

2-iodo-L-tyrosine
(2-IT)

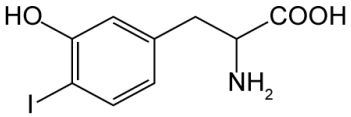

4-iodo-L-*meta*-tyrosine
(4-I-*m*-Tyr)

C

Group I.

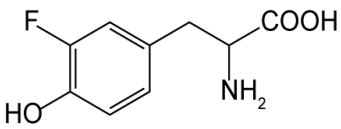

3-fluoro-tyrosine
(3-FT)

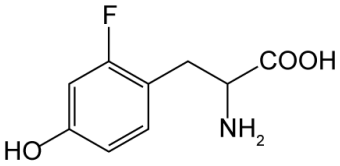

2-fluoro-tyrosine
(2-FT)

Group II.

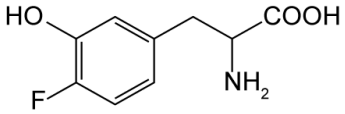

4-fluoro-*meta*-tyrosine
(4-F-*m*-Tyr)

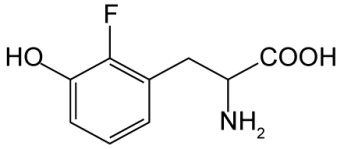

2-fluoro-*meta*-tyrosine
(2-F-*m*-Tyr)

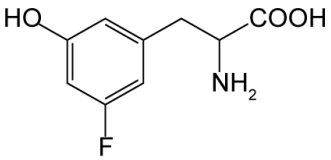

5-fluoro-*meta*-tyrosine
(5-F-*m*-Tyr)

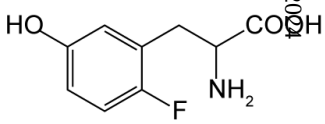

6-fluoro-*meta*-tyrosine
(6-F-*m*-Tyr)

Group III.

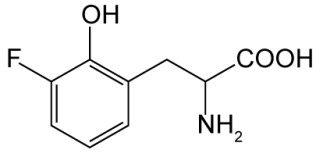

3-fluoro-*ortho*-tyrosine
(3-F-*o*-Tyr)

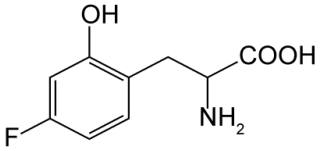

4-fluoro-*ortho*-tyrosine
(4-F-*o*-Tyr)

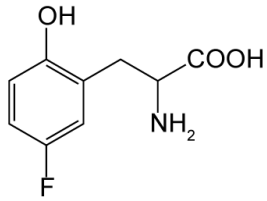

5-fluoro-*ortho*-tyrosine
(5-F-*o*-Tyr)

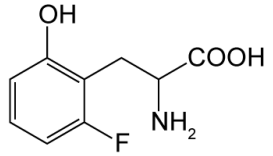

6-fluoro-*ortho*-Tyrosine
(6-F-*o*-Tyr)

Figure. 1

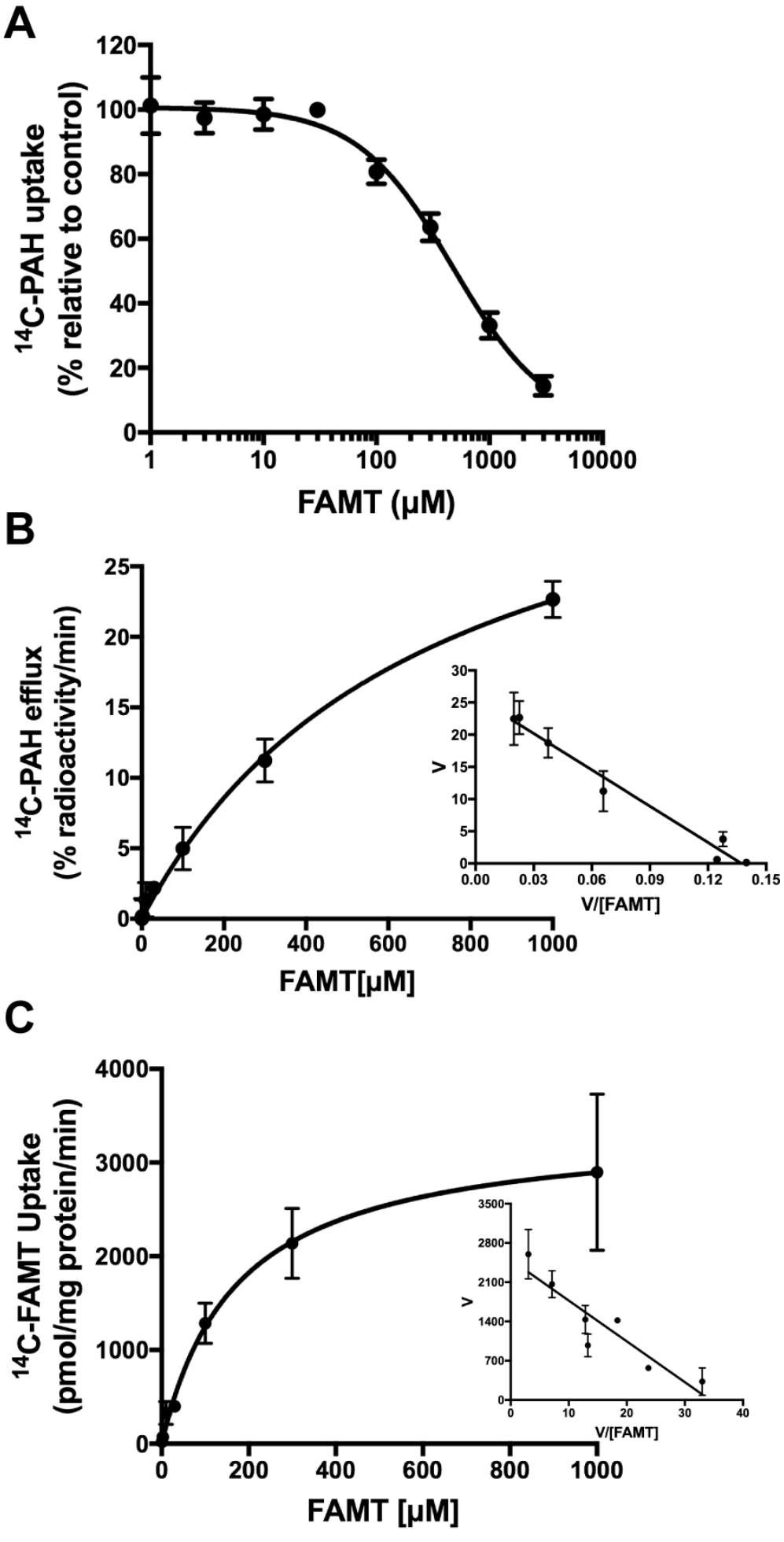

Figure. 2

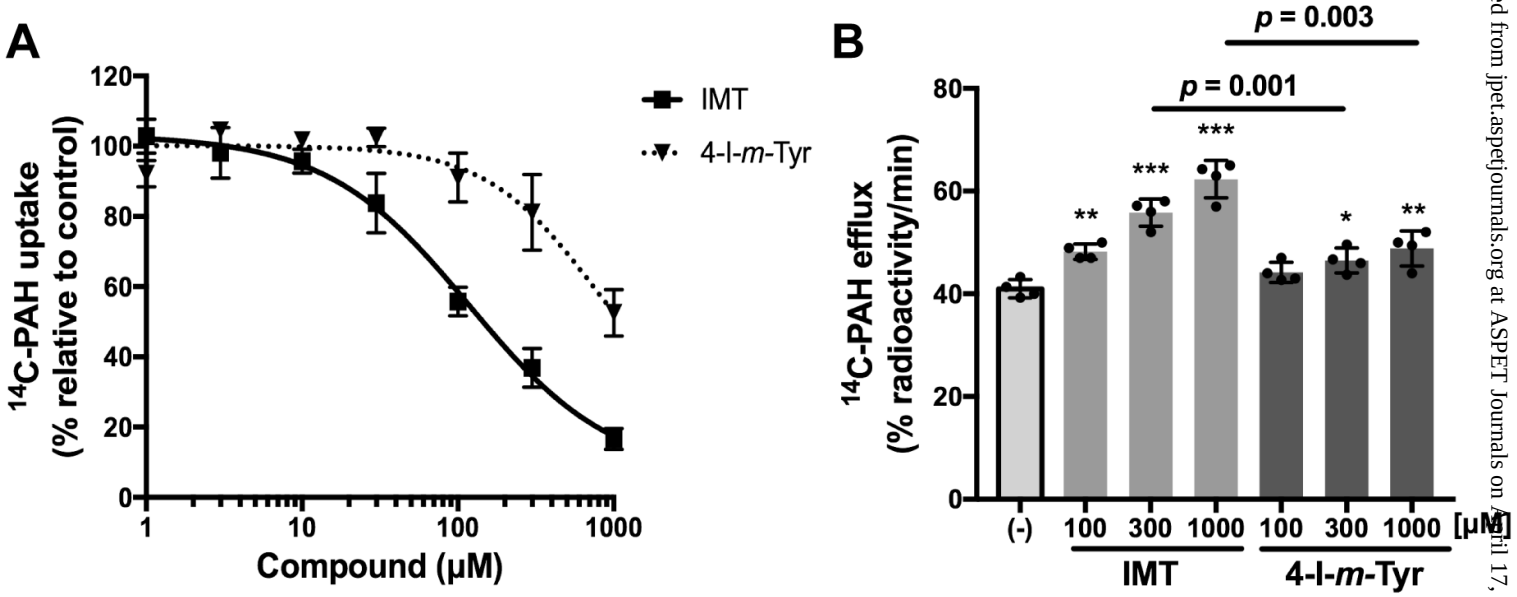

Figure. 3

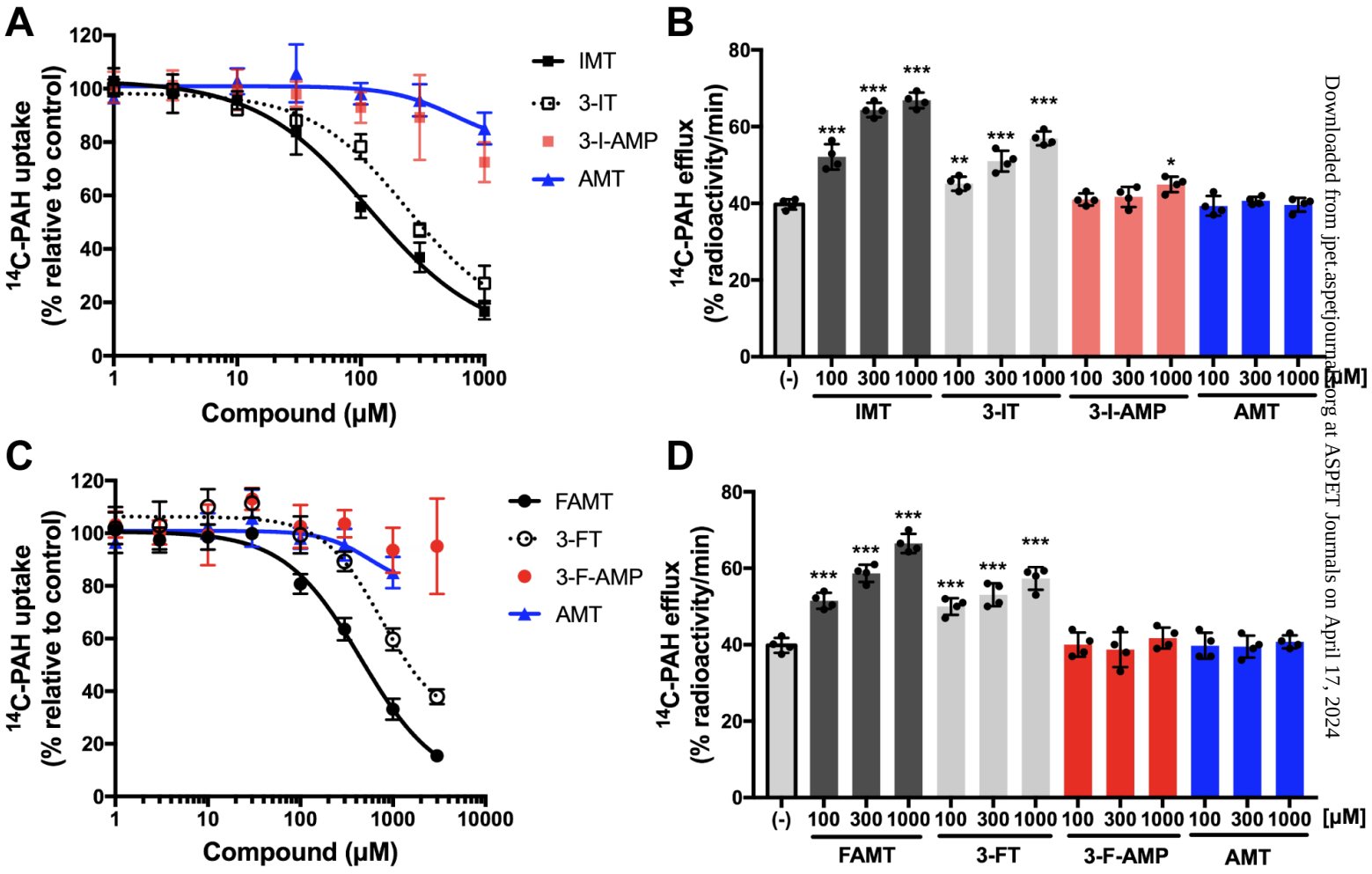

Figure. 4

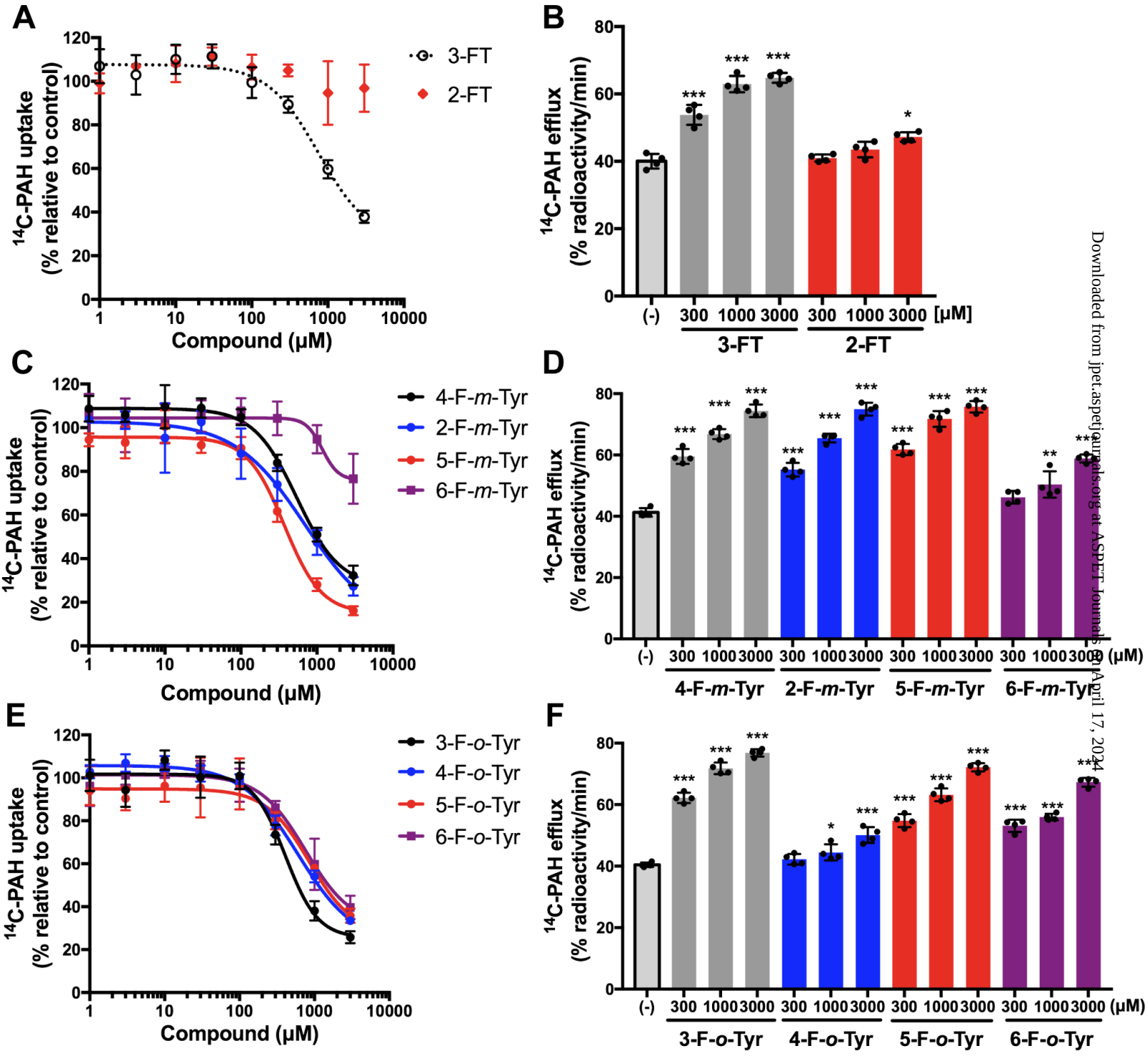

Figure. 5

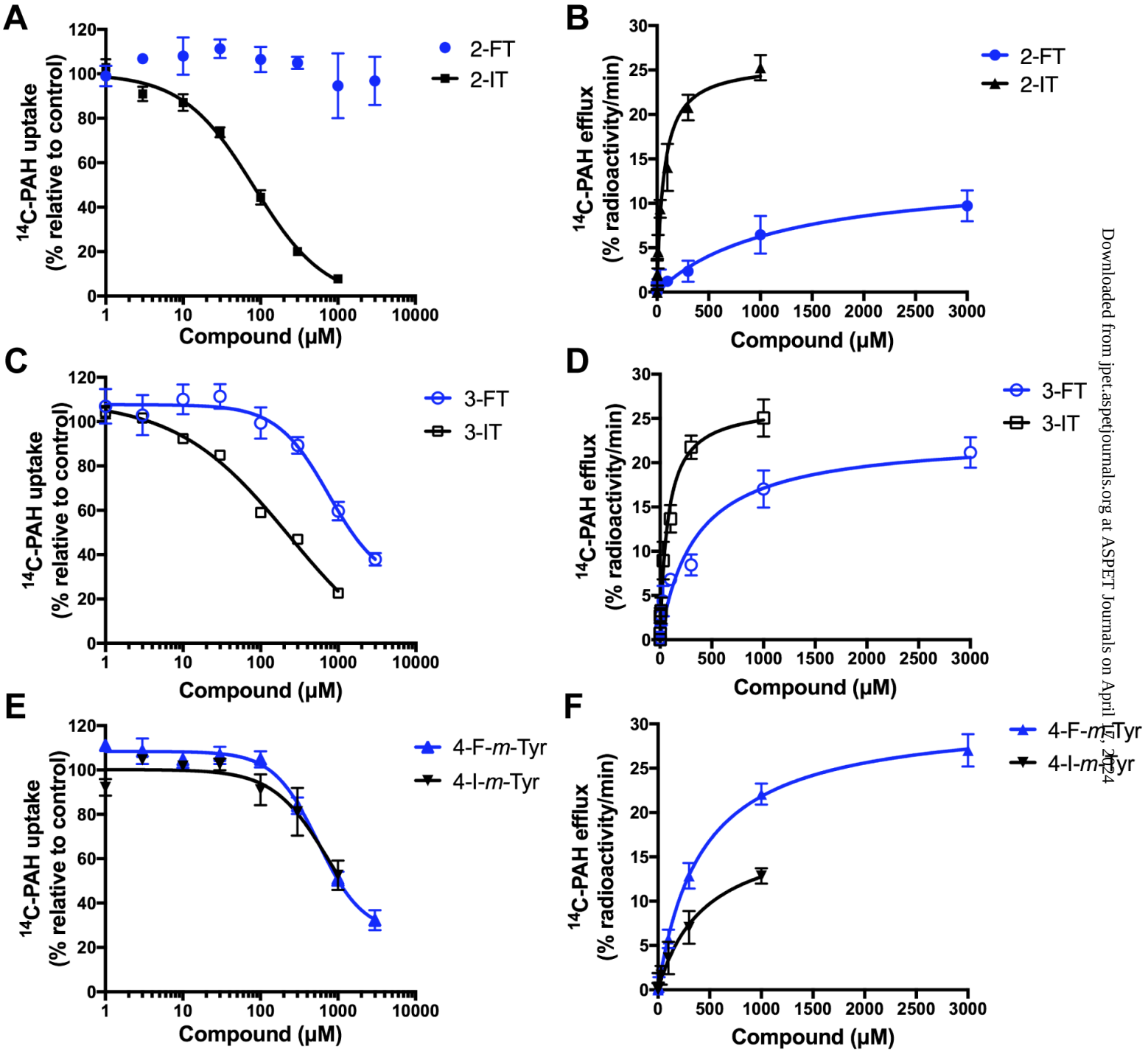

Figure. 6

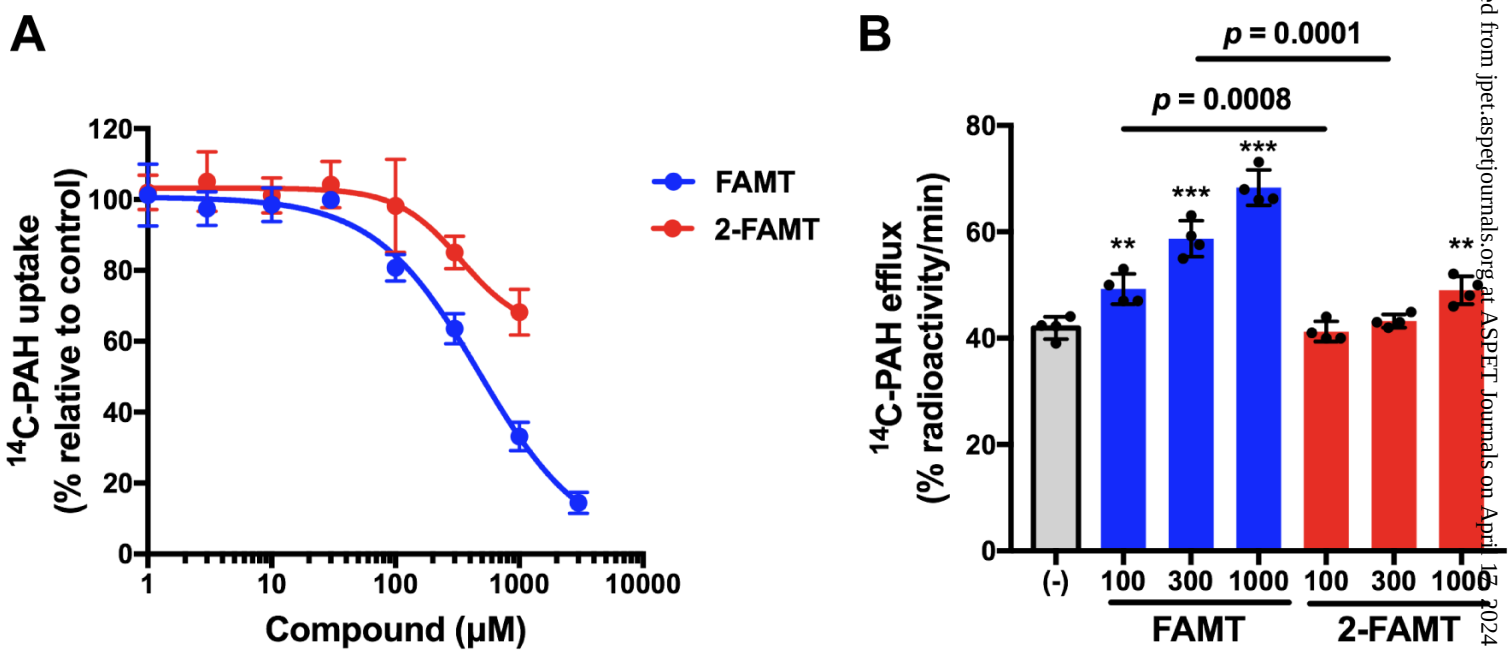

Figure. 7

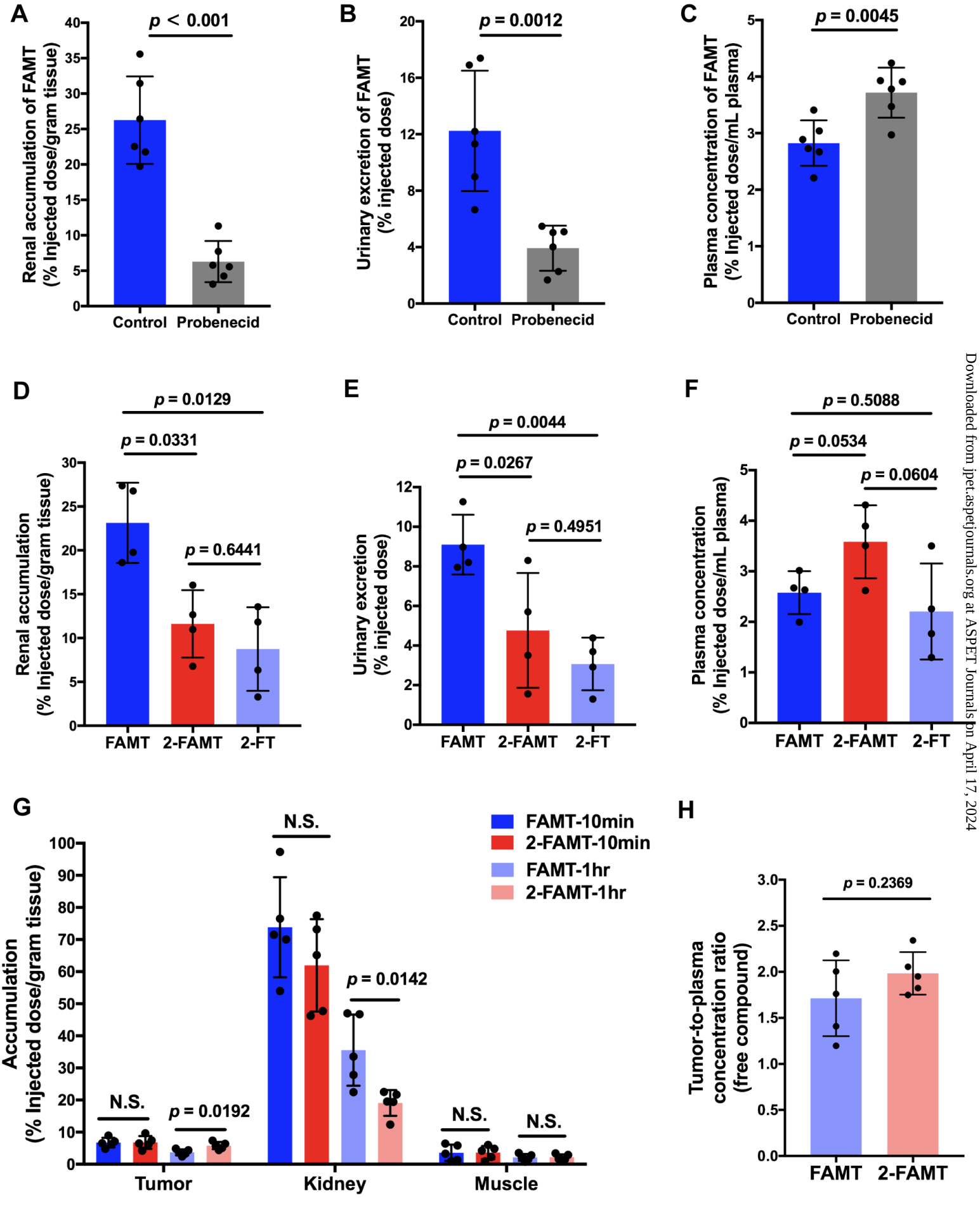

Figure. 8